RECRYSTALLIZATION
IN
SUPER - PURITY Al - 1.0% Mn ALLOY

by

ANJAN MAJUMDAR

DEPARTMENT OF METALLURGICAL ENGINEERING

INDIAN INSTITUTE OF TECHNOLOGY KANPUR

MAY, 1986

RECRYSTALLIZATION
IN
SUPER - PURITY Al - 1.0% Mn ALLOY

A Thesis Submitted
in Partial Fulfilment of the Requirements
for the Degree of

MASTER OF TECHNOLOGY

by

ANJAN MAJUMDAR

to the

DEPARTMENT OF METALLURGICAL ENGINEERING
INDIAN INSTITUTE OF TECHNOLOGY KANPUR
MAY, 1986

ME-1986-M-MAJ-REC

DEDICATED

TO

MY PARENTS

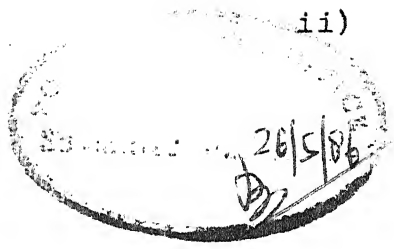

CERTIFICATE

This is to certify that the thesis entitled, 'Recrystallization in Super-purity Al-1.0% Mn Alloy' has been carried out by Mr. Anjan Majumdar under my supervision and that the work has not been submitted elsewhere for a degree.

May, 1986

(T.R. Ramachandran)
Professor & Head
Department of Metallurgical Engg.
Indian Institute of Technology
KANPUR-208016

ACKNOWLEDGEMENTS

The author here takes the privilege of expressing his deep gratitude and indebtedness to Dr. T.R.Ramachandran for his efficient guidance and constant encouragement throughout the course of the work at I.I.T. Kanpur failing which the present venture would not have been successful. The author also expresses his deepest-felt gratitude to Dr.K.P.Gupta for his guidance and valuable suggestions regarding the 'texture' part of the investigation.

The author is grateful to Dr. A.M. Gokhale for providing him with important suggestions in various matters related to the thesis work.

The author conveys his sincere thanks to his friends M/S. R.K. Bhattacharyya, R. Nakkalil, A. Bag and M.Sardar for their ever cooperating attitude and timely assistance.

The author is grateful to Mr. Mukherjee and Mr. Pal for their kind help in day to day experimental work.

The author wishes to express his gratefulness to Mr.V.P. Sharma and Mr. B.K. Jain for efficient printing and tracing respectively.

Lastly, the author deeply acknowledges the effort put by Mr. U.S.Mishra in quick typing of the thesis with amazing efficiency.

-ANJAN MAJUMDAR

CONTENTS

ABSTRACT

In the present investigation the recrystallization behaviour of Superpurity Al-1.0% Mn alloy has been studied by transmission electron microscopy and texture analysis, employing samples subjected to solution treatment and precipitation treatment. The precipitation treatment has been given at 400°C for 2h after the solution treatment at 620 for 24 h. The alloy has been deformed to 40%, 60% and 90% followed by annealing at 250°C, 300°C and 350°C for 1 h each. The nature of the precipitate particles has been found to be $MnAl_6$ by electron diffraction pattern analysis. The solution treated alloy shows higher recrystallization temperature compared to the precipitation treated alloy. This has been attributed to the simultaneous occurrence of recrystallization and precipitation processes in case of the solution treated alloy. The alloy shows varying texture on deformation with (111) [uvw], (110) [$\bar{1}12$], (123) [$41\bar{2}$] and (332) [$11\bar{3}$] orientations and almost random texture with a slight preference for (023) [$33\bar{2}$] orientation on recrystallization.

CHAPTER 1

INTRODUCTION

1.1 Aluminium-Manganese Alloys:

Manganese increases the corrosion resistance and improves the strength of the aluminium-manganese alloy. So it has been used since the beginning of the present century as a very common alloying element in aluminium (1).

The use of manganese as an iron corrector and corrosion improver was well-established by the early twenties and since then, aluminium-manganese alloys have been used both for castings and wrought products. Manganese in small amounts is also added to many of the medium strength aluminium alloys and to alloys containing a balanced amount of magnesium and manganese, which have gained strong popularity because of their good fabricability and high corrosion resistance.

There are two types of aluminium alloys that contain manganese: the ones in which manganese is the (or one of the) major alloying element and the ones in which manganese is only a minor addition. There are three types of wrought alloys that fall in the first category: 3003 which contains 1-1.5% Mn with no other major addition, 3004 where Mn and Mg are present in balanced amounts (typically 1-1.5% Mn and 0.8-1.3% Mg) and 3008 which is basically the 3003 alloy with

0.1-0.5% Zr. Zirconium improves stress corrosion resistance and high temperature strength of the alloy. In addition there are some casting alloys with upto 4% Mn or Mn plus Ni which are used especially for die casting. There is one more alloy: 3105 which contains Mn and Mg in almost equal proportion with little amount of chromium (Table 1.1).

Table 1.1 : Chemical Composition of Commercial Al-Mn Alloys

Alloy	Chemical composition in wt%
3003	Mn = 1.0-1.5%, Si = 0.6% max., Fe = 0.7% max., Cu = 0.05-0.20%, Zn = 0.10% max.
3004	Mn = 1.0-1.5%, Mg = 0.8-1.3%, Si = 0.3% max., Fe = 0.7% max., Cu = 0.25% max., Zn = 0.25% max.
3008	Same as 3003 with 0.1-0.5% Zr
3105	Mn = 0.3-0.8%, Mg = 0.2-0.8%, Si = 0.6% max., Fe = 0.7% max., Cu = 0.3% max., Cr = 0.2% max., Zn = 0.4% max., Ti = 0.10% max.

1.2 Aluminium-Manganese Equilibrium System:

The equilibrium diagram is shown in Fig.1.1. It can be seen from the diagram that manganese can dissolve into aluminium upto a maximum of 1.8% Mn at the eutectic temperature, the solubility decreasing with decreasing

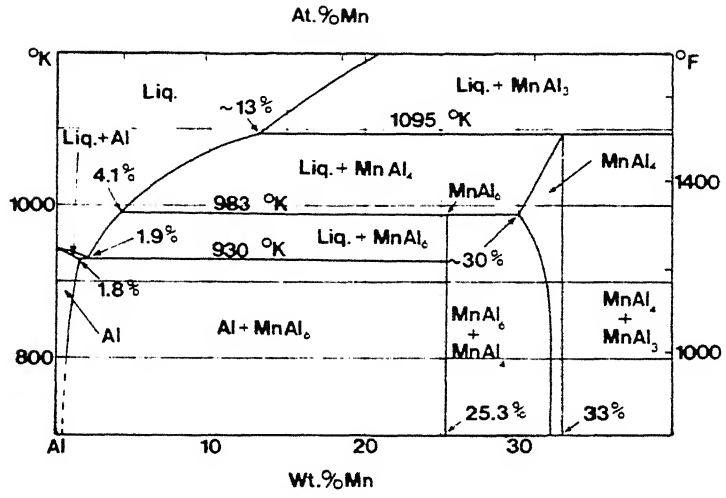

Fig. 1.1 : The aluminium end of the aluminium-manganese equilibrium diagram

temperature. The most probable values of the solid solubility are 1.8% Mn at 657°C, 1.00% Mn at 627°C, 0.42% Mn at 527°C and 0.20% Mn at 427°C. (2).

The eutectic Al-$MnAl_6$ is at approximately 1.9% Mn, 657°C. Unless it is rapidly cooled, it has a divorced structure, with the compound as the leading phase present as platelets, needles or skeletons (2).

The phase in equilibrium with aluminium is $MnAl_6$ (25.34% Mn) : orthorhombic, with lattice parameters a = 6.504 A°, b = 7.555 A° and c = 8.864 A°, density 3250 kg/m^3 and hardness Vickers 5400-5600 MN/m^2 (2). The $MnAl_6$ phase has a limited range of primary crystallization and it is formed by peritectic reaction at 710°C from the phase $MnAl_4$ (33.7% Mn). $MnAl_4$ is hexagonal, with lattice parameters a = 28.4 A°, c = 12.4 A° and hardness 7800 MN/m^2 (3). This phase is retained in alloys with more than 4-5% Mn, especially with rapid cooling. Several other phases are formed at higher manganese contents.

Aluminium-manganese alloy is not age-hardenable (4). This is because of the fact that precipitation from super-saturated solid solution of the alloy occurs at a reasonably higher temperature compared to other age-hardenable alloys. This is well indicated in the TTT curve for the Al-Mn alloy where the nose of the curve is at 500-550°C, whereas the nose for Al-Cu alloy is at 200°C. So after solution treatment

precipitation occurs at a temperature where the supersaturation of the Al-Mn solid solution is very low and hence the alloy shows little response to age-hardening treatment.

1.3 Properties of Aluminium-Manganese Alloys

1.3.1 Physical Properties: Manganese decreases the lattice parameter of aluminium solid solution. The lattice parameter decreases approximately linearly with the addition of manganese to reach a value of 3.996 A° at 15% Mn in solution (3). The electrical resistivity of the alloy increases linearly with increasing manganese content; the contribution to resistivity is ~ 3 μΩcm/wt% Mn (5). In contrast it has got insignificant influence on resistivity when present as $MnAl_6$ particles ~ 0.3μΩcm/wt%Mn (5). Manganese increases the density and magnetic susceptibility and decreases the thermal expansion co-efficient of the alloy.

1.3.2 Mechanical Properties: Aluminium-manganese alloys have got good strength and hardness. These properties improve with the addition of manganese, but ductility is affected to some extent (Table 1.2). Manganese in solution is most effective in increasing the strength rather than the case when it is present as undissolved intermetallic compounds (6). As a consequence of this dependence on dissolved manganese, the mechanical properties are strongly affected by freezing rate: the faster the rate the more manganese in

Table 1.2 : Mechanical Properties of Al and Al-Mn Alloys

Alloy	Freezing rate in °C/sec.	UTS in MN/m^2	Y.S. in MN/m^2	% Elongation
Al 99.99%		45	15	60
Al 99%		90	35	40
Al 99%+1%Mn		65	24	40
Al+1.25% Mn (comm.)	< 1	110	41	35
Al+1.25% Mn (comm.)	10^2	160	70	15
Al+1.25% Mn (comm.)	10^4-10^5	180	160	5

solution and higher is the strength.

During casting manganese tends to segregate into the liquid last to solidify, which collects at the grain boundaries and interdendritic spaces (7). If homogenization and subsequent working is not sufficient to diffuse the segregation of manganese and manganese rich zones persist, then it gives light striations since this zone is more resistant to etching. This is a structural feature of Mn-bearing alloys and known as 'light phenomenon.' It does not have any important effect on properties.

Fatigue resistance depends greatly on the location and distribution of manganese (7) : with the manganese in solid solution the resistance increases appreciably; a lesser increase results if it is present as well distributed, small, rounded compound crystals. But, if the compound is present as large, sharp cornered particles, then there is an appreciable decrease.

High temperature strength increases by the addition of manganese. However, above 2%, manganese tends to form large primary crystals (7) and its beneficial effect is greatly reduced.

Creep resistance of aluminium is increased substantially by manganese, but the effect is much less in alloys in which other elements are more effective. The alloy with 1.25% Mn has a resistance almost double that of 99.5% purity Al (8).

The modulus of elasticity and rigidity increase almost linearly by manganese additions. But with the addition of manganese, the damping capacity of aluminium decreases (8).

1.3.3 Corrosion Resistance: Aluminium-manganese alloys have got good corrosion resistance properties. Manganese compounds formed in aluminium have electrolytic potential that differ by only few mV at most from the potential of

aluminium. The phase $MnAl_6$ that is present in aluminium-manganese alloys has got an electrolytic potential of -0.85 V which is equal to the electrolytic potential of Al. Thus aluminium-manganese alloys are not susceptible to inter-granular or stress corrosion. This similarity of potential also means that pitting corrosion is limited (9). The effect of manganese is appreciable in severe corrosive conditions, less in milder.

Manganese is reported as a valuable addition to reduce corrosion by mercury (10) when aluminium comes in contact with mercury, it dissolves into it and an amalgam is formed. The aluminium finely dispersed in the amalgam readily reacts with the water vapour in the atmosphere and transforms to hydroxide. The process continues until either aluminium of water vapour is exhausted. When manganese is present in aluminium it hinders the wetting by mercury and thus reduces corrosion.

1.4 Application of Aluminium-Manganese Alloys: This alloy is one of the oldest and is produced all over of the world. Its good formability, corrosion resistance, weldability and ability to take good finishes, together with its somewhat higher strength than aluminium, make it a favourite for a variety of uses (11). The alloy is used mostly in the form of sheet, plate or foil.

One of the most extensive applications is for food handling equipment, such as cooking utensils, beverage cans and any other similar applications in which corrosion resistance as good as pure aluminium, absence of food contaminants and a somewhat better strength and stiffness than pure aluminium are needed. Another extensive use is in the building industry as siding and roofing. Corrugated sheet has been extensively used for buildings, airplane hangers, skyscrappers and lining of tunnels.

The food industry also uses aluminium-manganese alloys containing magnesium when strengths higher than those obtainable with the aluminium-manganese alloys are needed : two of the typical applications being the highest grade of cooking utensile and cans for beer and other beverages. The alloys with lower manganese and magnesium contents are used extensively in the automotive industry.

1.5 Purpose of the Present Investigation

In the present investigation recrystallization behaviour of the superpurity Al-1.0%Mn alloy has been studied. The alloy has been cold worked to various extent followed by thermal treatments at 250°C, 300°C and 350°C. The texture developed has been studied by X-ray diffraction and the microstructures, after various treatments, have been studied by transmission electron microscopy. The nature of the precipitating phases has been established by selected area electron diffraction, and their effect on the

deformation characteristics and recrystallization behaviour of the alloy has been studied.

CHAPTER 2

LITERATURE REVIEW

2.1 Deformation

Heidenreich (12) first showed, by electron microscopy, that the regions inside the grains of deformed high purity aluminium are broken up into units which he described as an arrangement of slightly misoriented 'crystal domains'. These are now usually referred to as 'cells'. Very low amounts of deformation (less than 5% for most metals) produce random slip-line traces on the thin foil electron micrographs but as the deformation is increased a greater number of dislocations is produced and a definite cell structure is formed. The average cell diameter is usually of the order of 1-3μm . The main features of the cell structure in fcc metals have been found to be as follows (13): i) the cell size is independent of the initial grain size and decreases to a limiting value after a certain strain. ii) the limiting value of the cell size increases with the softness of the metal and iii) the width of the cell walls increases with the hardness of the metal.

The cell interiors are relatively free from dislocations, whereas the walls are regions of high dislocation density. It has been found that although many of the cell walls are arranged irregularly, there is nevertheless a general tendency for them to lie parallel to low index

planes. Alignment along the {100}, {110} and {111} planes is very common in aluminium and many other fcc metals (14). The dislocation arrangements within the cell walls are complex and are often associated with loops (13). Weissman et al. (15) noted that the misorientation across the cell walls, in aluminium, is small when the cell structure is first formed and it increases with the increase in deformation. Also an increase in deformation is found to cause a decrease in cell size in case of fcc metals.

The sharpness of the cell walls formed during plastic deformation varies from metal to metal in a manner which correlates with the stacking fault energy. A cell structure results from the ability of screw dislocations to cross-slip out of their original planes and to arrange themselves in very localized regions which form the walls or relatively strain-free cells (16). Such an effect clearly occurs in a comparatively easy manner in metals of high stacking fault energy and so cell structures are usually found in aluminium alloys.

A number of investigations have been carried out on the effect of deformation on solid solution alloys. Gay et al. (17) reported that solid-solution elements reduced the size of the cell formed during deformation. From the investigation of several other workers it is possible to conclude that an increase in the solute content leads to a decrease in stacking fault energy which in turn influences

the formation and size of the cells. The behaviour of solid-solution alloys based on solvents having an inherently high stacking fault energy is less clearly understood. In the case of aluminium alloys this arises because of the low solubility of most elements at room temperature, and the need for quenching from an elevated temperature. Such quenching treatment introduces large numbers of defects (e.g. vacancies) into the structure with the consequent formation of dislocation loops which interfere with the normal processes of cell formation (18). It has been found that the strain required to form a cell structure in a quenched metal is greater than that for a slowly cooled one, since the moving dislocations interact with vacancies to produce jogs which decrease their mobility.

When second-phase particles are present in the matrix, then their size and spacing determine the dislocation distribution after cold work. The dominant parameter appears to be the size of the particles. Swann (14) has shown that widely-spaced coarse particles, in aluminium-copper alloys, promote the formation of a cell structure since they act as dislocation sources. Conversely, the effect of fine particles (i.e. less than 1000 A° in dia.) appears to be to inhibit the development of a cell structure during deformation. In this case the deformation required to initiate a cell structure is usually greater than in the corresponding single-phase metal and the cell size is

smaller for any given strain (18). Furthermore, the dislocation density is increased, as compared with single phase metal and a larger proportion of dislocations are situated inside the cells. Deformation structure of Al-1.04% Mn alloy has been studied by Gatto et al. (19). They carried out the precipitation-treatment at 560°C for 48 hrs (after the solution-treatment at 620°C for 80 hrs.) to get a dense dispersion of $MnAl_6$ particles and observed weaker cell structure compared to the solution-treated samples after same percent deformation. They attributed the result to the hindering effect exerted by the $MnAl_6$ particles on the process of cell formation.

Deformation bands have been found to be formed in different materials after cold deformation. Bay and Hansen (20) observed deformation bands in the grain interiors with an orientation spread $\geq$ 15° about the foil normal after 15 and 30% deformation in case of commercially pure aluminium. They found the width of the bands to be less than approximately 20μm and the number of deformation bands to be dependent on the degree of deformation, the number increases with increase in the degree of deformation. They observed grain boundary bands with a rotation spread $\geq$ 15° in fine grained 30% cold-rolled specimens . The structure of the grain boundary bands is rather similar to that of deformation bands in the grain interiors, being generally comprised of relatively narrow bands of a width less than

approximately 12 μm situated parallel and adjacent to some of the grain boundaries. The bands consist of elongated subgrains and show cumulative misorientations, in some cases with a large orientation stored across the band. Bay and Hansen (20) found the number of grain boundary bands to be smaller than that of deformation bands. The grain boundary bands are believed to be formed to accommodate the strain in certain grain boundary areas.

In cold rolled Cu-0.6% Cr, in addition to deformation bands another type of bands forming certain angles with rolling direction have been observed by Grewen et al. (21) and they described it as shear bands. Shear bands are considered to be deformation defects consisting of regions of intense localized plastic flow. They are believed to be caused by a materials inherent propensity for localized plastic flow.

Dillamore (22) reported the presence of transition bands in deformed metals. Transition bands are regions of high lattice distortion which result from inhomogeneous deformation in metals.

2.2 Recovery and Recrystallization

Recovery is the stage which occurs just before recrystallization during annealing after deformation. It usually refer to those changes which do not involve the

sweeping of the deformed material by migrating high angle boundaries. Thus, in this stage, a deformed crystal retains its basic identity, although the density and distribution of defects within it change. Recrystallization is the collective term applied to those stages in which the crystal orientation is altered by the passage of high-angle grain boundaries through the material. It includes the nucleation of new strain-free grains and their subsequent growth at the expense of the deformed material.

The primary recrystallization process depends on the extent of the deformation in the metal prior to annealing. This is because the driving force, for the process, is provided by the high internal energy associated with the deformed state. There is a minimum strain below which recrystallization does not occur and increasing the strain above this value lowers the temperature of the recrystallization limit. The recrystallization characteristics of deformed metals also depend on the deformation temperature and the initial grain size of the material. It has been found that lowering of deformation temperature causes a decrease in both the temperature and the effective overall activation energy of the start of primary recrystallization. Similarly, finer grain size materials recrystallize at a lower temperature compared to the coarser grain size materials. This is because finer grain size materials have higher dislocation densities (since dislocation density is inversely

proportional to the initial grain size) and consequently have lower activation energy required for recrystallization. The lower recrystallization temperature found in finer grain size materials can be interpreted in a different way, by the fact that grain boundary area is greater in this case and so nucleation becomes easier. But the distribution of deformation (and therefore of dislocations and internal energy) becomes more homogeneous as the strain increases. Hence, differences in grain boundary area will have a less marked effect, and consequently the various recyrtallization parameters will become less dependent on the original grain size, as the strain is increased.

More experimental work has been carried out on aluminium based solid solutions than on any other individual metal solvent, presumably because of its extreme sensitivity to the effects of impurities. A number of scientists investigated the effect of controlled additions of elements on recrystallization characteristics of aluminium. They found that almost all the solutes increase the recrystallization temperature — manganese, iron and chromium each raises the recrystallization temperature by about 200°C and silicon, copper and magnesium do so by less than 100°C (23). These investigators interpreted the observed recrystallization delay in terms of solute/grain boundary and solute/dislocation interactions which are reported to be playing main role in increasing the activation energy necessary for grain

boundary movement. They also suggested that the degree of recrystallization delay caused by a specific solute would be dependent on the elastic interaction between the solute/grain boundaries, which in turn is a function of the relative atom sizes of solute and solvent. Several workers have reported that the recrystallization process, after first being retarded by alloying additions, can ultimately be accelerated by greater additions of an alloying element. They attributed the higher composition acceleration of recrystallization to the increased strain resulting from comparatively large alloy additions.

Recrystallization behaviour of Al-Mn alloys has been studied by a number of investigators. Gatto et al. (19) have studied recrystallization behaviour of Al-1.04 Mn containing all the manganese in solid solution in one case and a dispersion of precipitate particles in the other. One part of the material was solution treated at 620°C for 80 hr. in order to obtain a single-phase alloy and the other part was precipitation treated at 560°C for 48 hr. after the solution treatment to get a dense dispersion of $MnAl_6$ precipitates. Then they were rolled at room temperature to various degrees of deformation ranging from 10 to 90% followed by annealing at different temperatures. The salient observations are: (i) cell structures occur at lower deformation and develop more regularly and homogeneously in the solution treated specimens than in those

containing precipitate particles and (ii) when the amount of deformation is small recrystallization occurs at higher temperature in specimens subjected to precipitation anneal; the effect is reversed for large deformation (Fig.2.1). The enhancement of recrystallization kinetics in precipitation treated samples after heavy deformation and in solution treated samples after low deformation has been attributed to the hindering effect played by precipitate particles and solute atoms respectively on subgrain boundary migration. Solute atoms play the role by forming a cottrell atmosphere around dislocations constituting the boundaries. It depends on the density of solute within this atmosphere which falls sharply with increasing temperature. It has been found that the temperature at which the cottrell atmosphere fades out is about 450°C. So in all cases where recrystallization temperature is shifted above 450°C (low deformation range), it is seen that recrystallization occurs more easily in solution treated samples; when the recrystallization temperature is below 450°C (high deformation range), the case becomes just the reverse.

Grain boundary migration occurs during recrystallization. Grain boundary migration can be defined as the movement of a grain boundary perpendicular to its tangent plane and it occurs when the boundary is subjected to a force large enough to cause its motion. The movement results in a reduction of free energy. The force comes from the removal of stored energy of deformation (as in primary

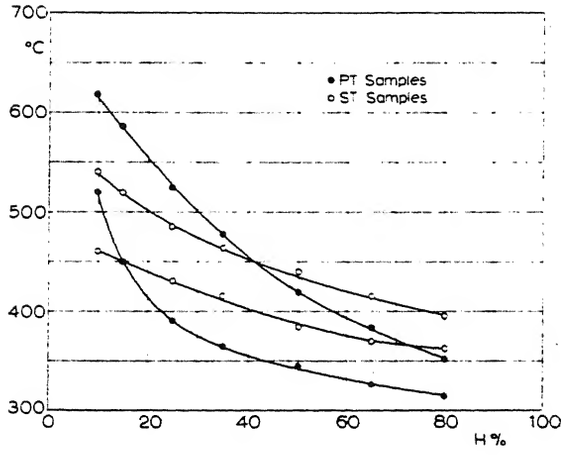

Fig. 2.1 : Plot of recrystallization beginning and end temperatures vs. percent deformation.

recrystallization) and the reduction of grain boundary area (as in grain growth). The principal advantage of recrystallization is the high driving force available. By controlling the amount of prior deformation, the driving force can be controlled. Grant et al. (24) observed that grain boundaries are able to migrate with widely varying velocities; low angle boundaries migrate much more slowly than the high angle boundaries.

2.3 Effect of Particles on Recrystallization

It is well established that a fine particle dispersion inhibits both the grain nucleation and growth rates while coarse particles ($> 1\,\mu m$ dia.) stimulates the nucleation rates by acting as nucleation sites. The inhibition of nucleation for finer particle dispersions has been attributed to the Zener drag on the cold-worked dislocation sub-structure. A similar drag effect on the freshly formed grain boundaries is also assumed to be responsible for the reduction in the grain growth rates.

The effect of fine particle dispersion on recrystallization has been studied by Nes (25). He found that the fine particle dispersion exerts a drag on the migrating sub-boundaries trying to stabilise the sub-grain structure and thereby inhibiting the nucleation of grains.

But large second phase particles may stimulate the nucleation of recrystallization in deformed metals. The

particles are important in both affecting the deformation structure and in providing an interface during annealing (26).

It has been recognized that the strain incompatibility of a rigid inclusion in a deforming matrix will result in the high dislocation densities and large lattice mis-orientations necessary for recrystallization. Investigators have found that at the larger particles small lattice rotations ($\lesssim 1^{\circ}$) may occur. It is favoured by large particles and strains. Humphreys (27) made an effort to measure the lattice misorientation from diffraction patterns of a number of areas each of diameter 0.6 μm, in the vicinity of a particle in Al-Si alloy and he plotted this misorientation as a function of distance from the particle surface (Fig.2.2). It can be seen that at large distances from the particle the orientations lie within a band of $\sim 10^{\circ}$, but at distances less than $\sim$ 4 μm (the particle dia.) larger mis-orientations upto 35° occur.

The interactions between dislocations and particles are complex. For the comparatively simple case of an alloy Al-Si containing well separated, strong, equiaxed particles in a single crystal deforming predominantly on one slip system at low temperatures, the dislocation structures produced near particles at which voids do not form are shown in Fig. 2.3 (28). The formation of large local lattice rotations is seen to be favoured by large particles and strains.

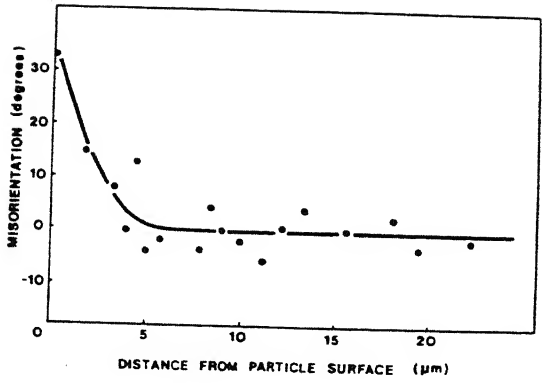

Fig. 2.2 : The orientation of the matrix in the vicinity of a particle.

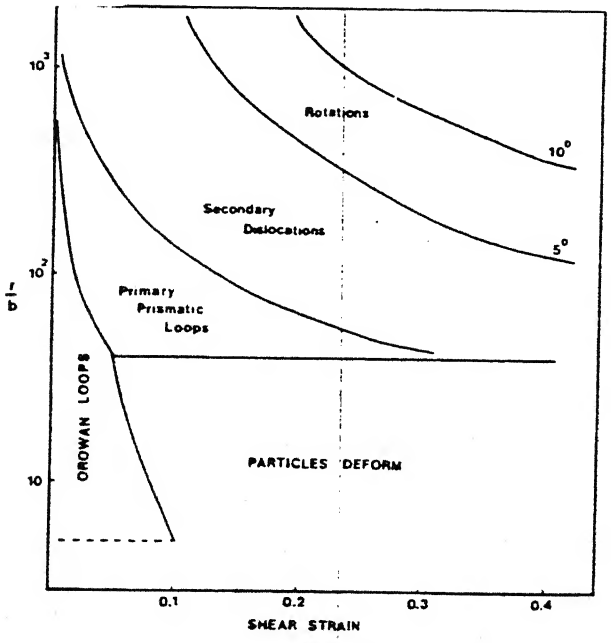

Fig. 2.3 : Deformation mechanisms at particles as a function of shear strain and particle radius (r).

The basic differences which exist between the deformation microstructures in particle free and particle containing materials originate from an interference with free movement of dislocations in particle containing alloys. Extensive studies of different alloy systems, mainly deformed to low total strains, have shown that small particles stimulate both dislocation loop formation and an increased frequency of cross slip (29). On a more microscopic level, such distribution of particles are known to promote a more uniform and fine scale distribution of slip (30).

Humphreys (27) studied the nucleation of recrystallization at second phase particles in deformed aluminium. The salient observations are (i) nucleation of deformed single crystals of aluminium alloys containing non-deformable particles of varying size but constant interparticle spacing is more rapid for crystals with larger particles, the nucleation rate being increased more than the growth rate, (ii) particle stimulated nucleation occurs above a critical particle size of 1-2 μm for a 95% reduction, the critical size increasing with decreasing deformation, (iii) when particle stimulated nucleation occurs, the final grain size is closely related to the interparticle spacing, (iv) a deformation zone is formed in the vicinity of particles which contains high dislocation density and lattice misorientation, (v) nucleation originates at pre-existing subgrains within the deformation zone and (vi) nucleation occurs by a rapid polygonization process involving sub-boundary migration.

Chan and Humphreys (31) investigated the effect of particle stimulated nucleation on orientation of recrystallized grains in an Al-6% Ni alloy containing a volume fraction of 0.1 of 1.1 μm diameter particles. They found the recrystallization to nucleate in the vicinity of the particles and the orientation of the recrystallization nuclei to be almost random, with the majority of the nuclei being misoriented by 15-45° from the adjacent matrix. This has been interpreted in terms of nucleation within the deformation zone at the particles.

2.3.1 Effect of Particle Size: For alloys containing widely spaced particles, the minimum size of particles at which recrystallization occurs is found to be ~1 μm in a variety of alloy systems studied by a number of scientists: Al-Si (27) and Al-intermetallic (20).

According to Humphreys (27), the critical particle size in Al-Si alloy increases as the strain is reduced (Fig. 2.4). The critical size refers to that particular particle size when recrystallization occurs very near to the particle. The number of recrystallization nuclei formed at a particle is also a function of particle size and this has been studied by several scientists. For particles in the size range 1-5 μm, usually only one grain is nucleated (27), but at particles larger than ~ 10 μm, multiple nucleation is frequently observed (20).

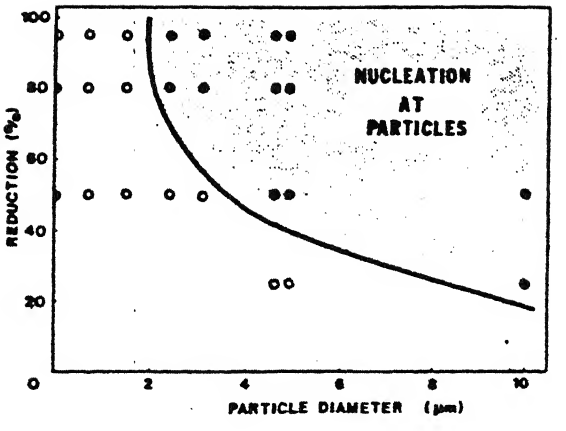

Fig. 2.4 : The conditions of strain and particle size for which recrystallization is nucleated at particles (27).

2.3.2 Effect of Particle Spacing: There is evidence that nucleation occurs preferentially at pairs or groups of particles even if the individual particles are below the critical size. This has been detected from in-situ annealing in the HVEM of deformed alloys by Porter and Humphreys (32). They found that during the annealing of deformed alloys of aluminium containing $\sim$ 10% volume of closely spaced sub-critical particles ($\sim 0.5\,\mu m$), recrystallized grains are formed near the group of particles.

2.4 The Deformation Zone

During cold working a region with high dislocation density is formed around the rigid particles. This region is known as the deformation zone. This is formed due to the misfit strains developed during the deformation. This deformation zone area extends to about a particle diameter from the surface of the particle into the matrix. The appearance of the deformation zone in aluminium alloys has been studied by Humphreys (27) and it is illustrated schematically in Fig. 2.5. Due to the operations of many slip systems it takes a spherical shape.

At small strains ($< 5\%$) dislocation loops are formed. At slightly higher strains the loops are no longer stable and instead dislocation tangles are formed. Gradually with increasing strain the distribution of dislocations around the particle becomes more homogeneous. In metals with a high

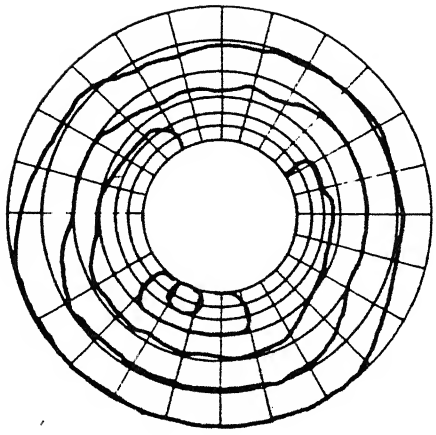

Fig. 2.5 : Schematic representation of the sub-structure in the deformation zone around a particle.

stacking fault energy a sub-structure is formed as in the rest of the material. Humphreys (27) found that the average sub-grain size in the deformation zone is consistently much smaller than in the rest of the matrix and the misorientation of the sub-grains relative to the matrix is large in particular close to the particle. It decreases with increasing distance from the particle and vanishes at a distance of about a particle diameter.

Sandstrom (33) proposed a model for the deformation zone. The model predicts that the width λ of the deformation zone measured from the particle surface is proportional to the particle diameter d

$$\lambda = \alpha d$$

where the constant α is about 0.8 and 1.0 for 50 and 95% cold reduction respectively for aluminium. This relation is in perfect agreement with the observations of Humphreys (27). Once the width of the deformation zone which is assumed to be spherically symmetrical is known its dislocation density can be evaluated from the amount of geometrically necessary dislocations in the zone.

Another importamt parameter is the maximum mis-orientation Θ_m across the deformation zone. With the help of a continuum mechanics model Humphreys proposed the following relationship

$$\Theta_m = \varepsilon d / 3 \lambda$$

where ε is the true strain of the cold reduction. For small

strains ~ 0.1 ($\lambda \sim 0.5$ d), θ_m is about $0.7\,\varepsilon$. For large strains $\varepsilon > 2$ ($\lambda \sim$ d), θ_m is about $0.3\,\varepsilon$. To obtain a maximum mis-orientation of atleast 10°, typical for a high angle boundary, the cold reduction must exceed 30%.

2.5 Formation and Growth of Recrystallization Nuclei Around Particles

The formation and growth of a recrystallization nucleus are assumed to take place in three stages (34). Firstly, the formation of a small sub-grain highly mis-oriented with respect to the matrix. Secondly, the growth of this nucleus within the deformation zone around the particles and thirdly, the growth of the nucleus away from the environment of the particle.

In order to ensure the survival of a recrystallization nucleus around a particle essentially two conditions must be fulfilled (33) -

(a) The nucleus must acquire high angle boundaries in the deformation zone; otherwise the growth rate of the nucleus will not be sufficiently large to compete with other forms of recrystallization. Initially no high angle boundaries can be expected to be present and subgrain coalescense must occur in order to generate them. However, since the subgrains are in general randomly oriented in the matrix this would be an extremely slow process and

is not of practical importance. For the formation of high angle boundaries within the deformation zone, the maximum misorientation across the zone θ_m must exceed typically about 10^{o} (34). This implies that the cold reduction must be larger than 30%.

(b) The critical size of the nucleus must be smaller than the total extent of the deformation zone. The most critical stage for the survival of the nucleus is in most cases when the nucleus has consumed the deformation zone and should continue to grow out into the matrix where the dislocation density is lower. For growth to continue the size of the nucleus must exceed the critical radius R_{cr} in the matrix where

$R_{cr} = 2\gamma_{max}./\tau\rho$, γ_{max}. = grain boundary energy per unit area, τ the dislocation line tension and ρ the dislocation density in the matrix.

2.5.1 Formation of a Nucleus by Subgrain Growth: Since no high angle grain boundaries are present initially in general they must be formed. This is assumed to occur by subgrain growth. Both coalescence and growth by boundary migration are assumed to be of importance for the subgrain growth. This stage of formation of nucleus is known as stage I.

The most probable situation is that a subgrain which is slightly larger than its neighbours grows at the expense of them. According to Sandström (35) this growth is controlled by the following equation:

$$\frac{dR}{dt} = \frac{11}{2} \alpha_1 M\tau \left[\frac{1}{R_m} - \frac{1}{R}\right]$$

where R and R_m are the radius of the largest and the average sized subgrain respectively, α_1 is a constant of about unity, M the climb mobility of the dislocations, and τ the dislocation line tension. It can be shown that the parabolic growth of the average subgrain size gives a parabolic time dependence for the size R of the potential nucleus ($R \alpha t^{1/2}$) (33).

At the same time as the subgrain grows its boundary misorientation increases. This is a consequence of the variation of the lattice orientation from the boundary of the deformation zone to the particle surface. When the boundary mis-orientation of the potential nucleus becomes sufficiently large, migration by high angle boundary processes becomes important; when they start to dominate, the transition to the next stage is assumed to take place.

2.5.2 Growth in the Deformation Zone: A nucleus formed in the deformation zone continues to grow by high angle processes. The growth can be described by the following equation:

$$\frac{dR}{dt} = \beta m \left[\bar{\tau} \rho_{dz} - \frac{2\bar{\gamma}}{R}\right]$$

where R is the radius of the nucleus, β a constant of about unity, m the grain boundary mobility, ρ_{dz} the dislocation density in the deformation zone, and $\bar{\gamma}$ the surface energy per unit area of the nucleus. The growth rate initially rises due to the increase of the m with increasing boundary mis-orientation. Once the high angle plateau has been reached, m is approximately constant and consequently also the growth rate. The growth continues in this way until the whole deformation zone is consumed. A transition now takes place from the second (growth inside the deformation zone) to the third stage (growth outside the deformation zone).

2.5.3 Growth Outside the Deformation Zone: When the nucleus has consumed the deformation energy of the deformation zone and obtained its size, the growth slows down due to the reduction of the driving force. The growth of the nucleus outside the deformation zone is controlled by the same processes as in stage II (38). The growth rate can be described by the equation

$$\frac{dR}{dt} = \beta m \left[\tau \rho_{matrix} - \frac{2\gamma}{R}\right]$$

where ρ_{matrix} is the dislocation density in the matrix. This is less than ρ_{dz} due to the fact that dislocation density in the matrix is less compared to the deformation zone and hence the surface energy term has a correspondingly larger influence on the growth rate. This results in a slower rate of growth in stage III.

The growth of a nucleus around a nondeformable particle is illustrated in Fig.2.6. The three stages of growth are easily identifiable. The subgrain growth in stage I gives a comparatively slow parabolic growth. The growth in stage II is considerably accelerated due to high angle processes. The vertical bar on the curves gives the position where the high angle plateau for the mobility is reached. Outside the deformation zone in stage III the growth rate is considerably smaller than in stage II due to the lower dislocation density. Fig. 2.6 also depicts the influence of the particle diameter on the growth rate. The growth rate decreases with increasing particle size initially and for longer time, as in stage III, the particle diameter has little influence on the nucleus size. However, if the particle size is sufficiently small, the nucleus will stop to grow when the deformation zone has been consumed.

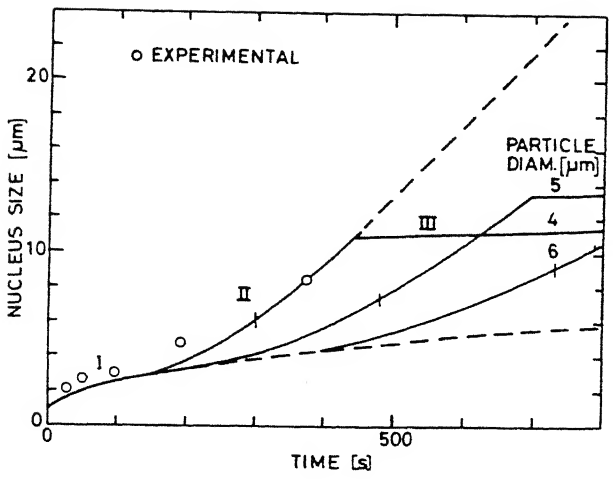

Fig. 2.6 : Diameter of recrystallization nucleus versus time for three different particle diameters 4,5 and 6 m (33)

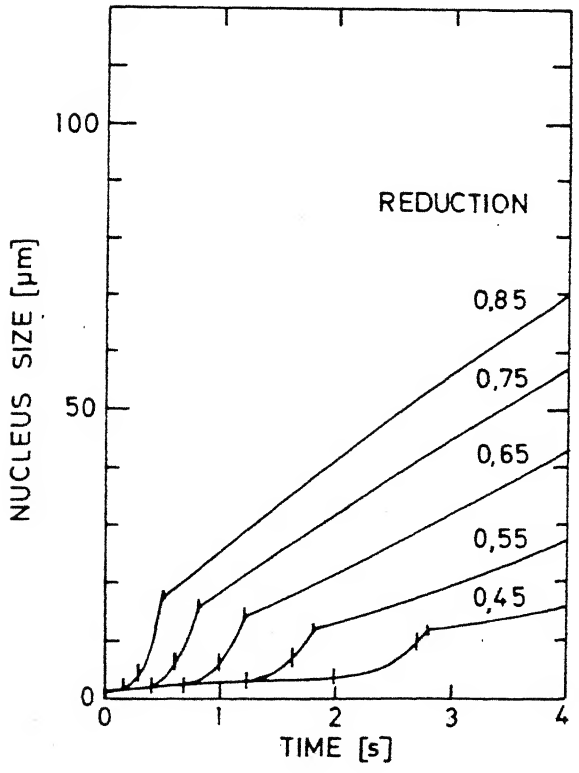

Fig. 2.7 : Diameter of recrystallization nucleus versus time for different % cold-deformation (33).

The effect of the amount of deformation on the nucleus size is illustrated in Fig.2.7. It has been found that the nucleus size increases quite rapidly as a function of the increasing cold reduction (33). All three stages of growth are affected. This is natural since the dislocation densities in the deformation zone and in the matrix, and the width of the deformation zone increase with the strain.

In certain cases high angle boundaries may have been formed already during cold working. Bay and Hansen (20) observed this in case of aluminium alloys. This is because dynamic recovery takes place at room temperature deformation for aluminium alloys. In such cases, the growth of nuclei may begin directly in stage II.

2.6 Texture

Each grain in a polycrystalline aggregate normally has a crystallographic orientation different from that of its neighbours. Considered as a whole, the orientations of all the grains may be randomly distributed in relation to some selected frame of reference, or they may tend to cluster, to a greater or lesser degree, about some particular orientation. Any aggregate characterized by this condition is said to have a preferred orientation or texture. It may be defined simply as a condition in which the distribution of crystal orientations is non-random.

In cold-rolled sheet, most of the grains are oriented with a certain plane (hkl) roughly parallel to the sheet surface, and a certain direction [uvw] in that plane roughly parallel to the direction in which the sheet was rolled. These are called deformation textures. Basically they are due to the tendency of a grain to rotate during plastic deformation.

When a cold-rolled metal or alloy, possessed of a deformation texture, is recrystallized by annealing, the new grain structure usually has a preferred orientation which is different from that of the cold-worked material. This is called an annealing texture or recrystallization texture. The development of recrystallization texture can be explained by two theories (36). In the 'oriented nucleation theory' recrystallization texture formation is solely attributed to a selection of certain orientations in the nucleation process. Once the grains have been nucleated, they are assumed to grow at the same rate, independent of their orientation. The 'oriented growth theory', on the other hand, assumes that the orientation of the nuclei is random and the growing grains undergo a selection process according to their different growth rates due to different crystal orientations.

The industrial importance of preferred orientation lies in its effect on the macroscopic properties of materials. Materials having preferred orientations are anisotropic, i.e.,

have different properties in different directions. Such properties are usually objectionable. But sometimes, the intended use of material requires directional properties and then preferred orientation is desirable. For example, the steel sheet used for transformer cores undergoes repeated cycles of magnetization and demagnetization in use, requiring a high permeability in the direction of the applied field. Since single crystals of iron are more easily magnetized in the [100] direction than any other, the rolling and annealing treatments given on the steel sheet are deliberately chosen to produce a high degree of preferred orientation in [100] direction.

2.6.1 Texture in Aluminium Alloys

Heye and Wassermann (37) have shown that the formation of rolling texture in fcc metals can be described by slip on the {111} <110> glide systems. Dillamore and Stoloff (38) tried to find the relationship between stacking fault energy and the texture developed in fcc metals. According to them, for low stacking fault energy materials crystal rotations result from deformation by a {111} < 112 > slip or twinning mode and for high stacking fault energy materials cross-slip predominates and crystal rotations resulting from slip on {111} < 110 > systems control the development of texture.

It has been seen that the rolling texture of aluminium is gradually changed from an orientation (123) $[41\bar{2}]$ to (112) $[11\bar{1}]$, as the reduction is increased. According to Dillamore and Roberts (39), the 'brass-type' texture (110) $[\bar{1}12]$ can only occur at small reductions in aluminium. Some authors (40) have found a 'brass-type' texture in pure aluminium with small additions of iron. It is claimed that the effect depends on high concentration of iron in solid solution.

Normally the recrystallization texture of aluminium is a mixture of cube texture, (100) [001] and (123) $[41\bar{2}]$. According to Bunk (40), the recrystallization texture is (12) $[41\bar{2}]$, when the rolling texture is of the 'brass-type'. But Lihl and Pexa (41) reported that a rolling texture, (123) $[41\bar{2}]$ was transformed to the cube texture after recrystallization and a 'brass-type' texture to (113) $[21\bar{1}]$. A different result has been reported by Sundberg (42). He found that the 'brass-type' texture was transformed to (110) [001] after recrystallization. Thus all the authors failed to find any general connection between the rolling and the recrystallization textures. Sundberg (42) concluded from his results, that the (110) [001] orientation is the main recrystallization texture as long as the rolling texture is of the 'brass-type' and for normal rolling texture, (112) $[11\bar{1}]$ in aluminium, the annealing texture is a mixture of the cube texture and complicated other

orientations of the rolling texture type.

Dons and Nes (43) reported the formation of cube texture on recrystallization of aluminium-alloys and they found that the strength of the cube texture component in commercial purity aluminium was influenced by a series of parameters: the iron and silicon content, the cold rolling reduction, the recrystallization temperature etc.

Chan and Humphreys (31) found the texture of an Al-6 wt% Ni after 95% cold deformation was similar to that of the deformed single phase aluminium except for the weakening of texture which they attributed to the effect of large volume fraction of the second phase particles. They observed randomization of texture after full recrystallization at 230°C for 17 hrs. Herbst and Huber (44) also reported random orientation of the recrystallized grains in aluminium alloys.

Bleck and Bunge (36) worked on the recrystallization and texture of an AlMn 1 alloy with one part of the alloy being solution-treated at 600°C for 24 hr. and the other part precipitation-treated at 400°C for 5 hr. after the solution-treatment. They found the rolling texture to be similar to that reported by other authors (42,45) for both the cases after 95% deformation. After recrystallization at high temperature the solution-treated alloy formed the cube texture and the orientation

distribution of the recrystallized grains in the precipitation-treated alloy was nearly random with only a slight preference of the rolling texture and cube texture positions. Grain growth after prolonged annealing had been found to enhance slightly the cube orientation with respect to the other orientations.

CHAPTER 3

EXPERIMENTAL PROCEDURE

3.1 Material Studied

The material studied in the present investigation is superpurity Al - 1.0% Mn alloy. The alloy has been received from the Alcan International, Kingston Laboratories, Canada in the form of 7 mm. thick plates.

3.2 Treatments

The 7 mm. thick plate has been divided into three parts — the first part rolled down to 4 mm., the second to 1 mm. and the third to 0.67 mm. thickness. All of them are then solution-treated at 620°C for 24 hrs. The treatment has been carried out in tubular horizontal electrically heated furnace. It enables the material to get rid of the previous deformation effects and to be present as a monophase alloy, because all the manganese would dissolve in aluminium at this temperature.

The solution-treated samples are then divided again into two parts — one part being preserved as such (henceforth referred to as solution-treated alloy) and the other part is given a precipitation treatment at 400°C for 2 hrs. (henceforth referred to as precipitation-treated alloy) in the same furnace. So for all three plates, there are two types of samples — solution-treated and

precipitation-treated.

Now both solution-treated and precipitation-treated samples of 4 mm, 1 mm and 0.67 mm thicknesses are rolled down to 0.4 mm. to obtain 90%, 60% and 40% reduction in thickness respectively. Rolling has been carried out in all the cases at room temperature.

The rolled samples are then annealed at different temperatures:

i) 250°C for 1 hr.

ii) 300°C for 1 hr.

iii) 350°C for 1 hr.

The annealing treatments are carried out in a salt bath with temperature controlled to $\pm$ 1°C.

3.3 Nature of Investigation

The following studies have been conducted on the alloy:

i) Deformation characteristics of the alloy in the solution-treated as well as precipitation-treated state,

ii) Recrystallization behaviour of the alloy in these two states and comparison between the two,

iii) Identification of the precipitates, measurement of their sizes and the effect of precipitates on recrystallization,

iv) Texture analysis of the cold-worked and recrystallized alloy in the solution-treated and precipitation-treated states.

Textures studies have been carried out in an ISO-DEBYEFLEX 2002D Diffractometer and all electron optical studies have been conducted in a Philips EM 301 electron microscope operated at 100 KV.

3.4 Electron Microscopy

3.4.1 Sample Preparation: After proper mechanical and thermal treatments the samples are chemically thinned down to 0.1 mm. thickness with the help of a chemical solution containing conc. H_3PO_4, conc. H_2SO_4 and conc. HNO_3 in the ratio 7:2:1 (by volume). The thinning is carried out at 70°-80°C. The chemically thinned samples are then subjected to electropolishing for the preparation of thin foils using window technique. The mixture of ethanol and perchloric acid (90:10 by volume) has been used as electrolyte. The electropolishing has been carried out at a voltage 13-16 V and current density 0.15-0.2 A/cm^2. The temperature is kept below 0°C with the help of liquid nitrogen.

3.4.2 Information from Electron Micrographs and Electron Diffraction Patterns: A number of electron micrographs

have been taken to study the morphology and size of the precipitates, size of the cells of the deformed structure and also to follow the changes of the deformed structure with annealing at different temperatures towards the completion of the recrystallization process. The nature of the precipitate has been established by analysing the electron diffraction patterns taken from the precipitates.

The size of the precipitate has been calculated from the following formula (46)

$$\bar{D}_s = \frac{3}{2} \pi \frac{A_A}{L_A}$$

where $\bar{D}_s$ is the mean size of the precipitate, A_A is projected area of the precipitate per unit area and L_A is projected perimeter of the precipitate per unit area of observation.

For the calculation of density of precipitates the foil thickness has been taken to be 2000 A°.

3.5 Texture Studies

For texture studies, all the samples have been taken of the same dimension - 25 mm x 15 mm x 0.3 mm. The surface layer has been removed by chemical polishing using the same chemical reagent used for the chemical polishing of electron microscopic samples.

The analysis has been carried out by using Schulz's

reflection method (47). The diffracted beam intensity is measured by the scintillation counter and displayed as counts. (111) poly figures have been drawn in all the cases from these counts.

CHAPTER 4

RESULTS AND DISCUSSION

4.1 Introduction

Electron microscopic studies have been carried out on the cold-worked as well as annealed alloy for both the solution-treated and precipitation-treated samples. Texture analysis also, has been done on cold-worked and recrystallized samples for both the treatments, with an intention to correlate this with the results obtained from the electron microscopic studies. Attempt has also been made to comment on the effect of precipitate particles on recrystallization and also on texture.

4.2 Texture Studies

Texture studies have been carried out on solution treated and precipitation treated samples by using Schultz's reflection method (47). The results obtained from the analysis are discussed below.

4.2.1 Solution treated Alloy: The textures obtained from the cold worked and annealed solution treated alloy are shown in Figs. 4.1 to 4.3.

Figure 4.1(a) shows the rolling texture of the 90% deformed solution-treated alloy. The (111) pole figure shows the rolling plane is very close to (111). In the

absence of the full texture plot it is not possible to determine the indices of the rolling direction.

Figure 4.2(a) exhibits the (111) pole figure of the same alloy after 60% cold deformation. The orientation is found to be of 'brass-type', (110) $[\bar{1}12]$ by comparing with the ideal orientation for the (111) pole figure. The occurrence of 'brass-type' texture in commercial aluminium alloys has been reported by Dillamore and Roberts (39) and also by Sundberg (42).

Figure 4.3 exhibits the (111) pole figure of the same alloy after 40% deformation. The component (332) $[11\bar{3}]$ is found to be the strongest one compared to other rolling components.

The rolling texture changes with the annealing of the alloy. Figs. 4.1(b) and 4.1(c) show the (111) pole figure of the 90% deformed alloy after annealing at 300°C and 350°C for 1 h each respectively. Fig. 4.1(b) shows the presence of the rolling texture component (111) [uvw] along with the other weaker component (023) $[33\bar{2}]$, while Fig.4.1(c) exhibits the presence of strong (023) $[33\bar{2}]$ component only. Fig. 4.2(b) exhibits the (111) pole figure of the 60% deformed alloy after annealing at 350°C for 1 h. It shows almost random orientation with a slight preference for the component (023) $[33\bar{2}]$.

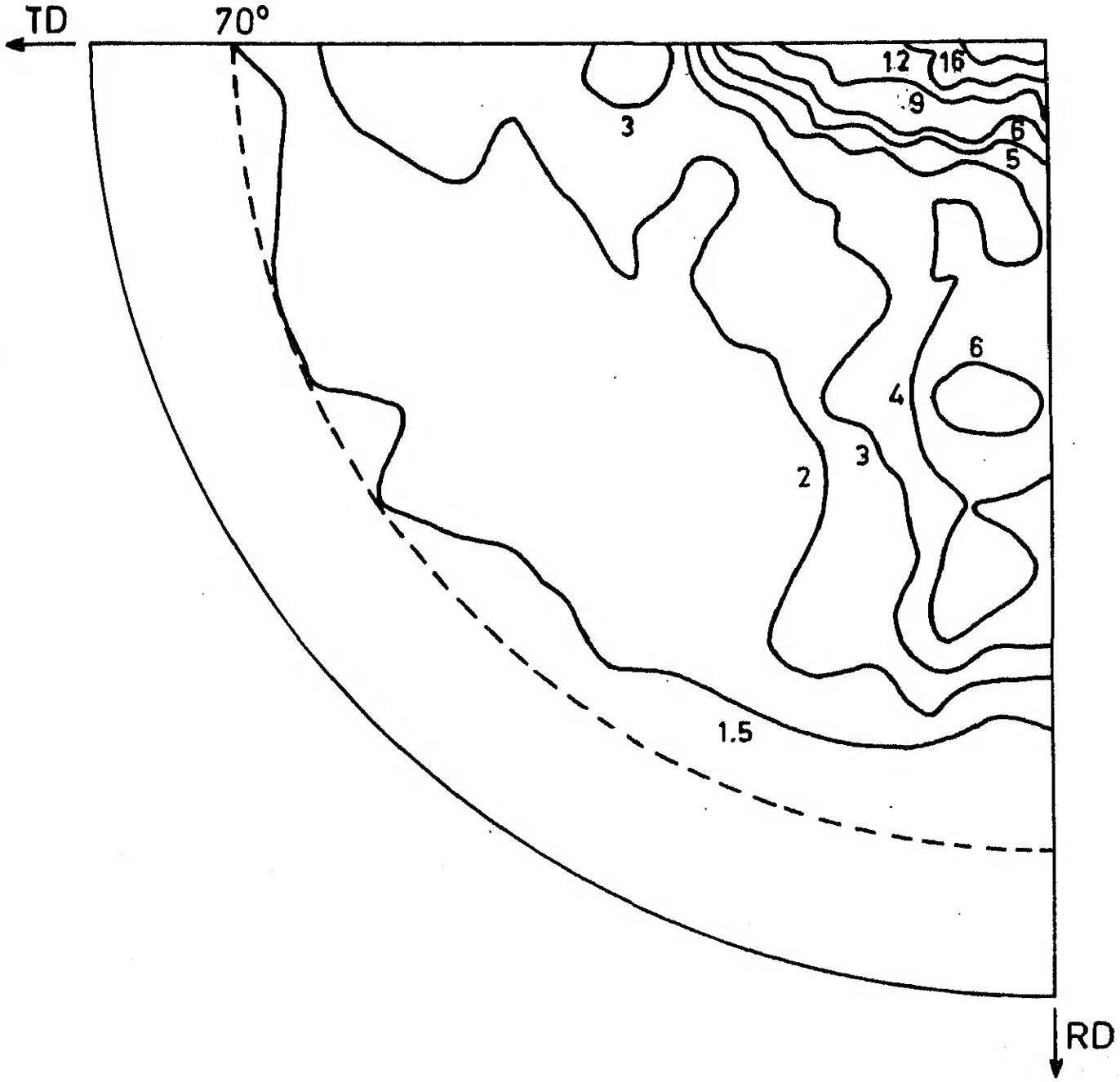

Fig. 4.1(a) (111) pole figure of solution-treated alloy, deformed 90 %.

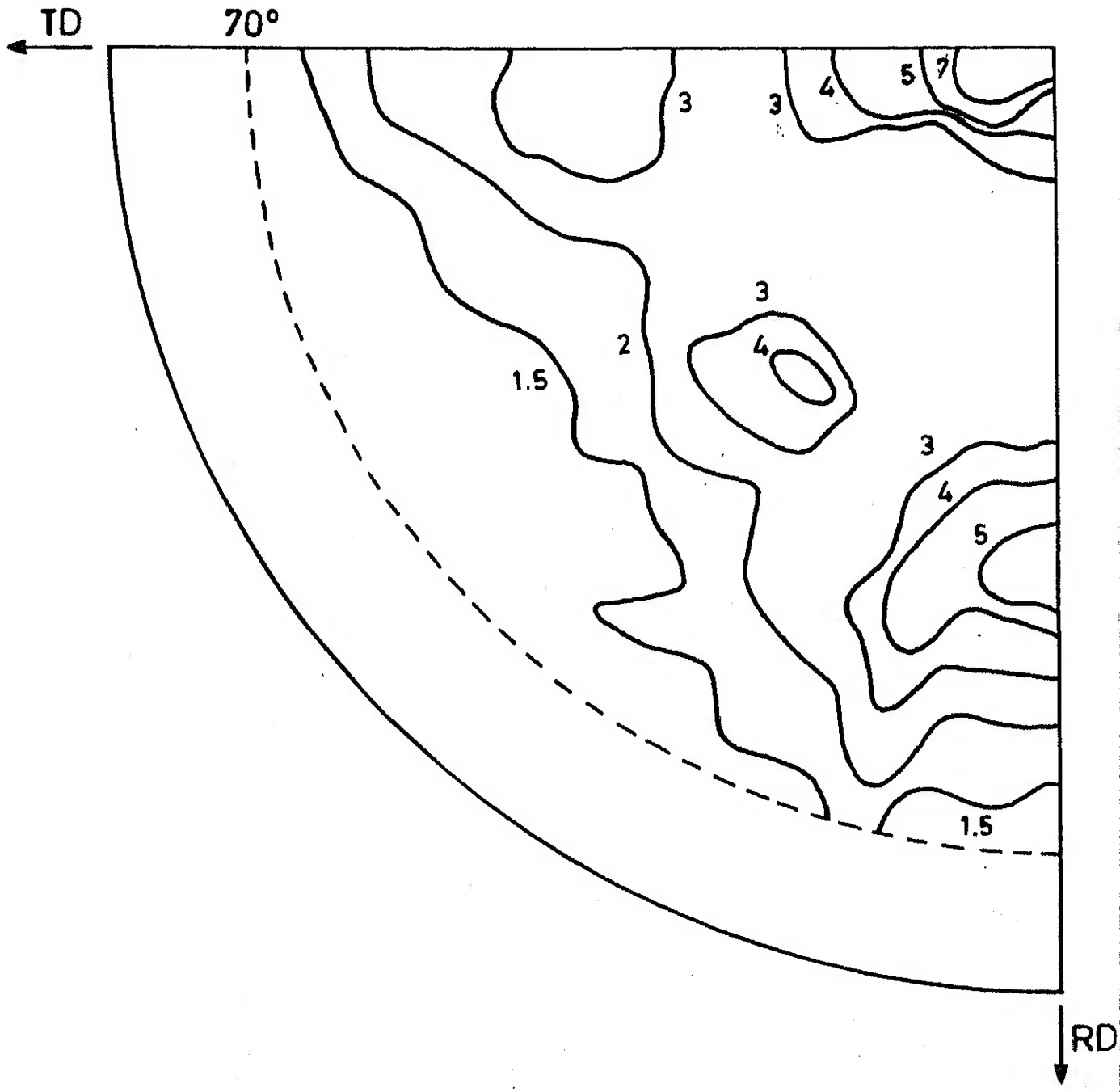

Fig. 4.1(b) (111) pole figure of solution-treated alloy, deformed 90% and then heated to 300°C for 1hr.

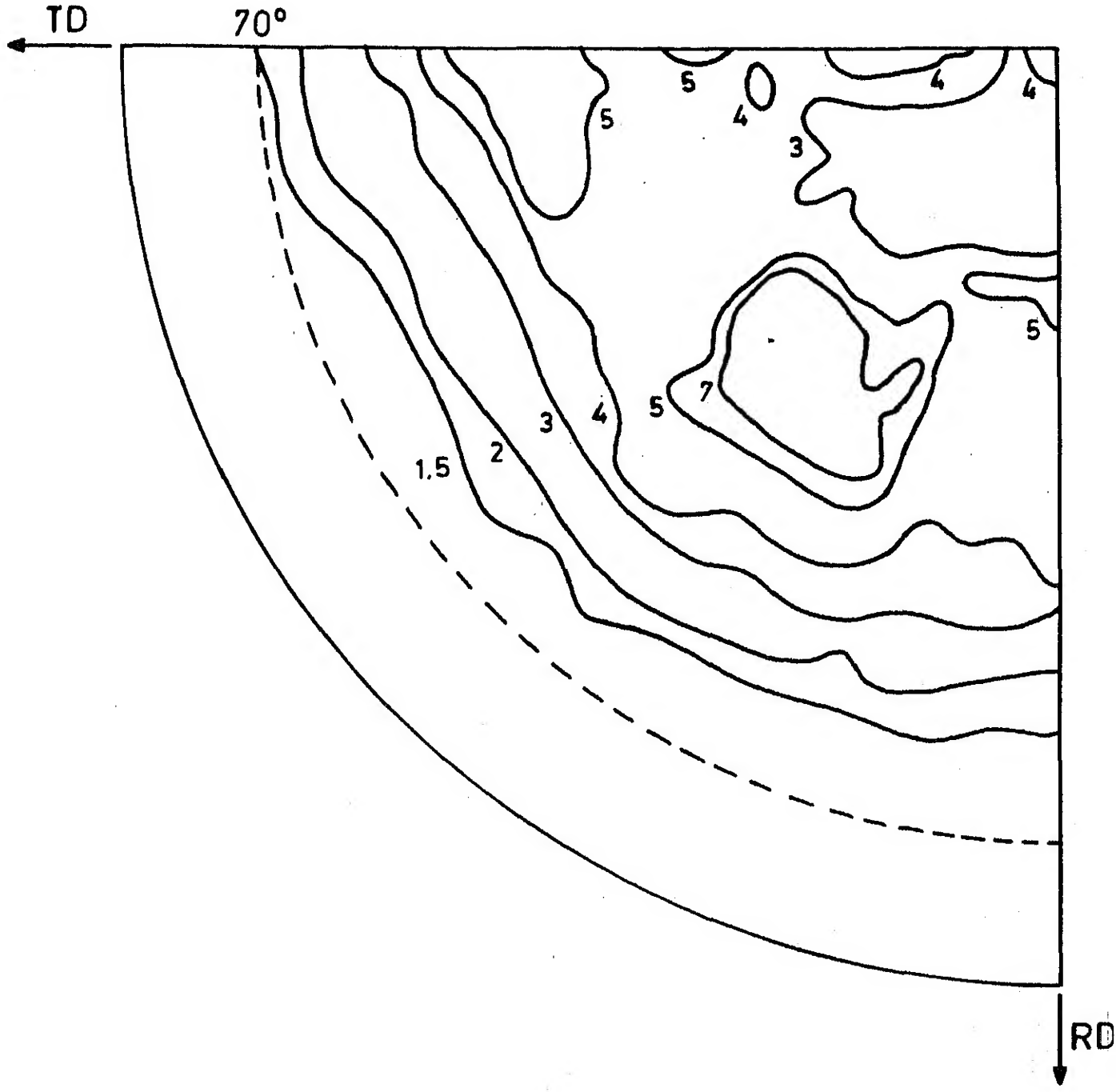

Fig.4.1(c) (111) pole figure of solution-treated alloy, deformed 90% and then heated to 350°C for 1hr.

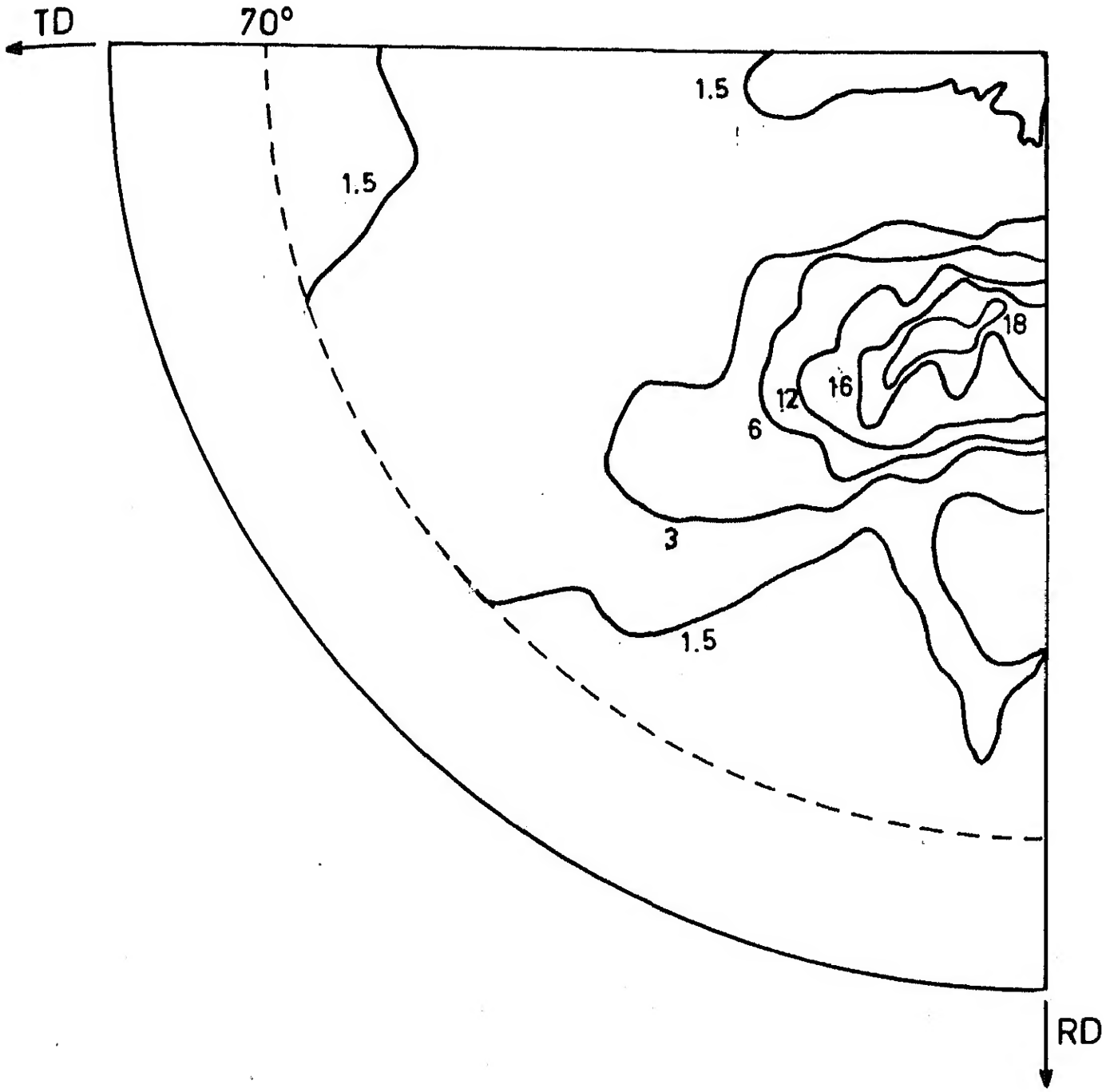

Fig. 4.2(a) (111) pole figure of solution treated alloy, deformed 60 %.

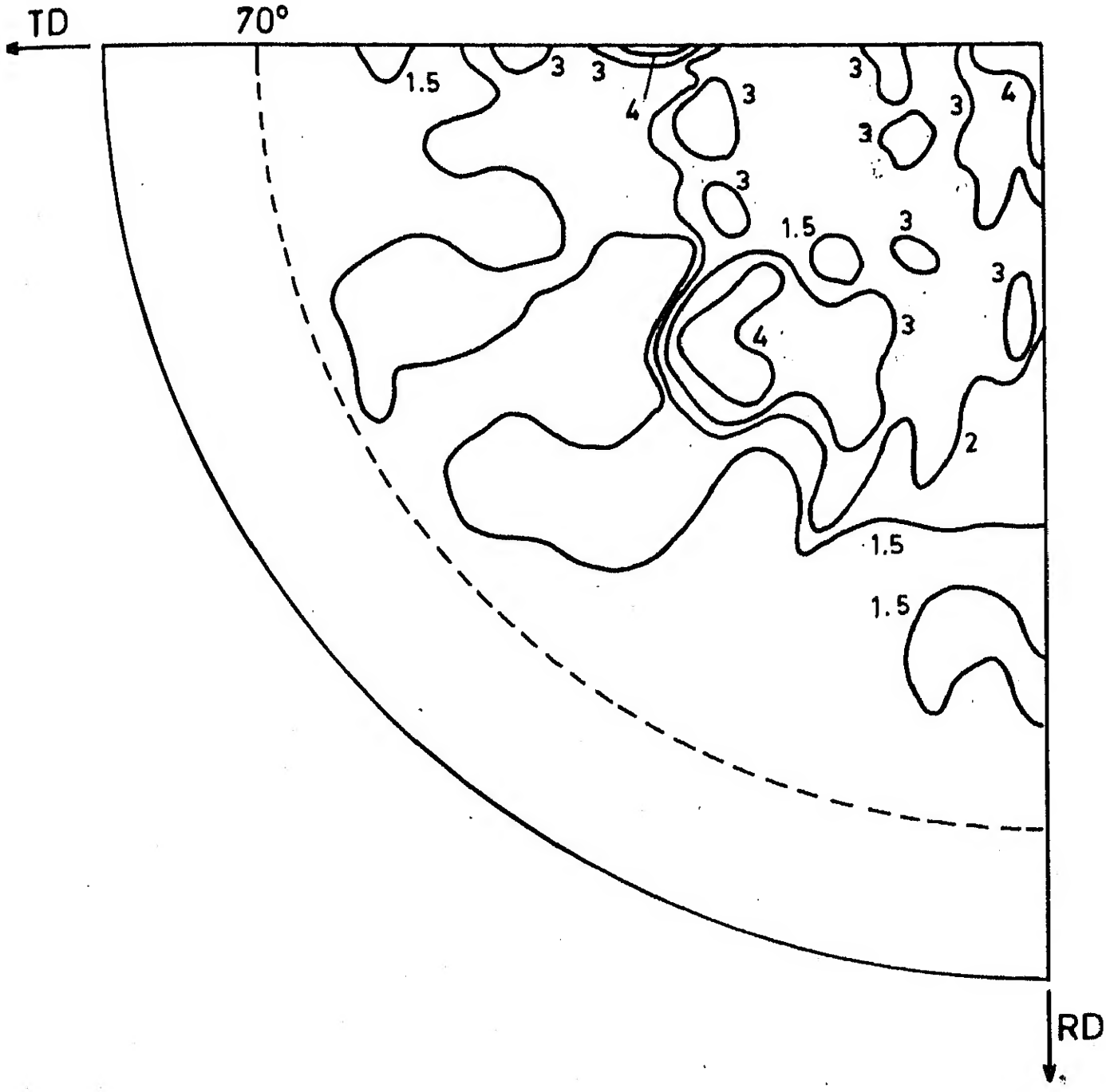

Fig. 4.2 (b) (111) pole figure of solution-treated alloy, deformed 60% and then heated to 350°C for 1hr

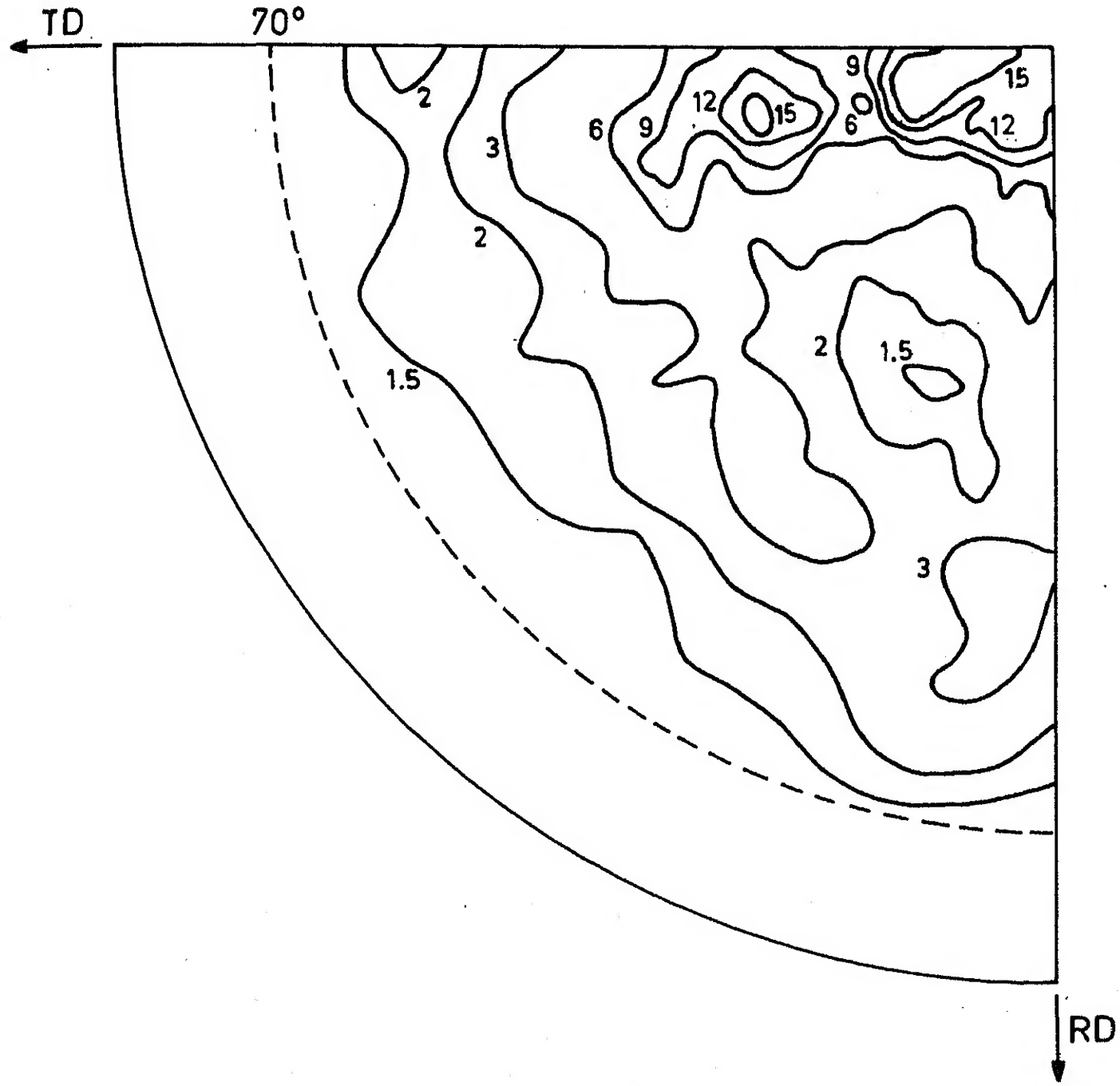

Fig. 4.3 (111) pole figure of solution-treated alloy, deformed 40%.

4.2.2 Precipitation treated Alloy: The textures obtained from the cold-deformed and annealed precipitation treated alloy are shown in Figs. 4.4 to 4.5.

Figure 4.4(a) shows the (111) pole figure of the 90% deformed precipitation treated alloy. The figure shows very close to (123) $[41\bar{2}]$ type of orientation. Fig. 4.5 illustrates very weak rolling texture of orientation (111) [uvw] for the same alloy, deformed 60%.

Bleck and Bunge (36) reported weaker texture for the precipitation-treated commercial purity aluminium alloy compared to the solution-treated alloy. They carried out the precipitation treatment at 500°C for 200 hrs. and the precipitates were of mean size $\sim 1.5\,\mu m$. The same type of weakening of texture has been observed by Chan and Humphreys (31) in a recent study. They observed weak rolling texture after 90% deformation in case of Al-6% Ni alloy containing particles of mean size $\sim 1.1\,\mu m$. The weakening of rolling texture by second phase particles is ascribed to the large volume of the material occupied by the deformation zones at the particles.

Due to the difference in orientation between the solution-treated and precipitation-treated samples after a particular percent deformation, it is not possible to compare the rolling texture of the alloy in these two states.

Figures 4.4(b) and 4.4(c) show the (111) pole figures of the 90% deformed precipitation-treated alloy after

annealing at 300°C and 350°C for 1h each respectively. The alloy shows (023) $[33\bar{2}]$ orientation after annealing at 300°C for 1h (Fig. 4.4b) and some what random orientation after annealing at 350°C for 1h (Fig. 4.4c).

It has been found in the present investigation that the 90% deformed solution-treated alloy exhibits strong (023) $[33\bar{2}]$ orientation after annealing at 350°C for 1 h. The same type of orientation is exhibited by the 90% deformed precipitation-treated alloy after annealing at 300°C for 1 h. The orientation becomes some what random when the material is annealed at 350°C for 1 h.

A comparison between the Figs. 4.1(b) and 4.4(b) illustrates the fact that the rolling component is still prominent in the 90% deformed solution-treated alloy after annealing at 300°C for 1h, while it is absent in case of 90% deformed precipitation-treated alloy after the same treatment. This is an effect believed to be caused by the particles and is attributed to the precipitation from the supersaturated solid solution at 300°C causing a hindrance for the subgrain boundary migration. This delays the recrystallization process and rolling component (111) [uvw] is retained by the 90% deformed solution-treated alloy even after annealing at 300°C for 1 h.

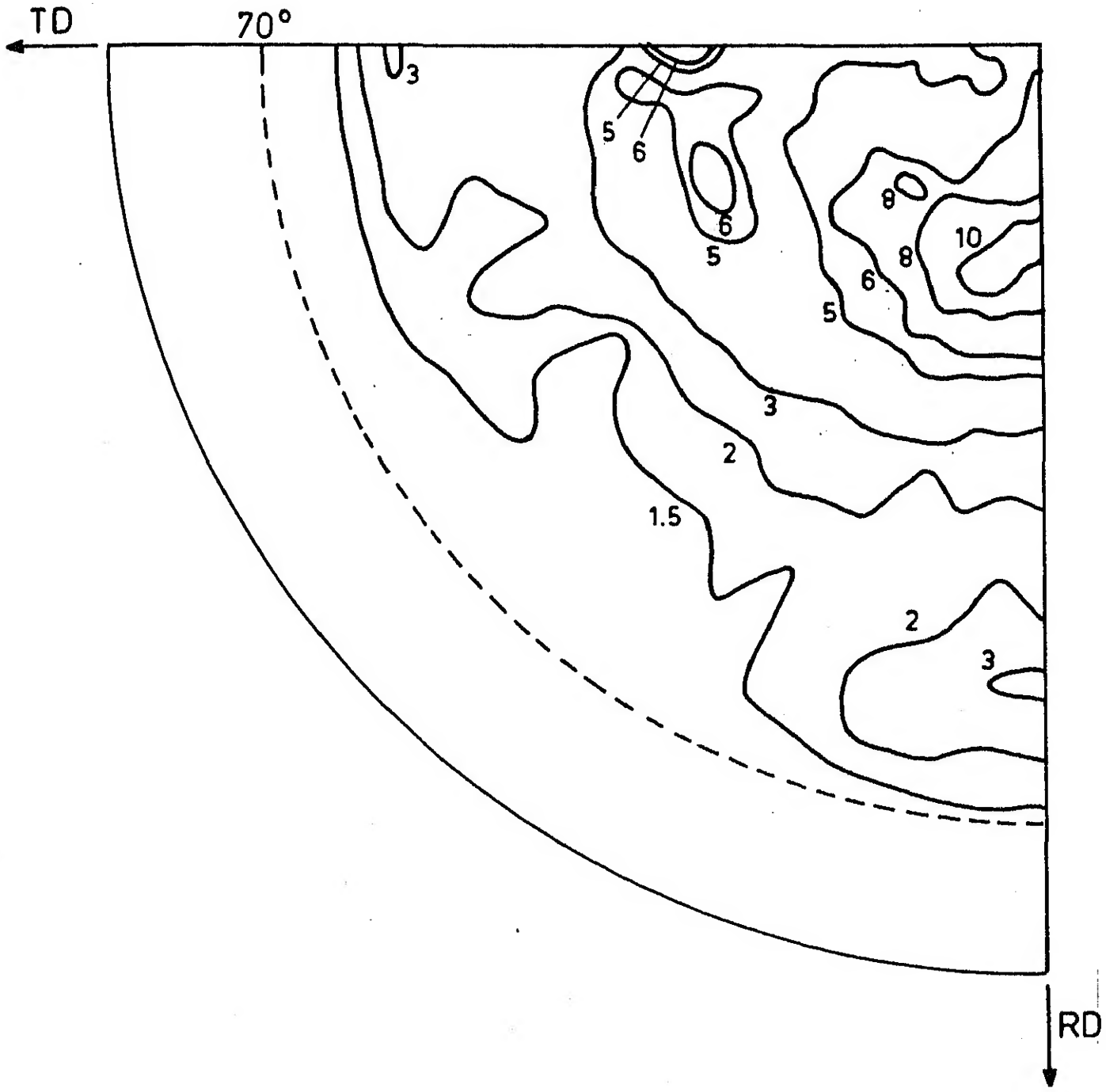

Fig. 4.4 (a) (111) pole figure of precipitation-treated alloy, deformed 90%.

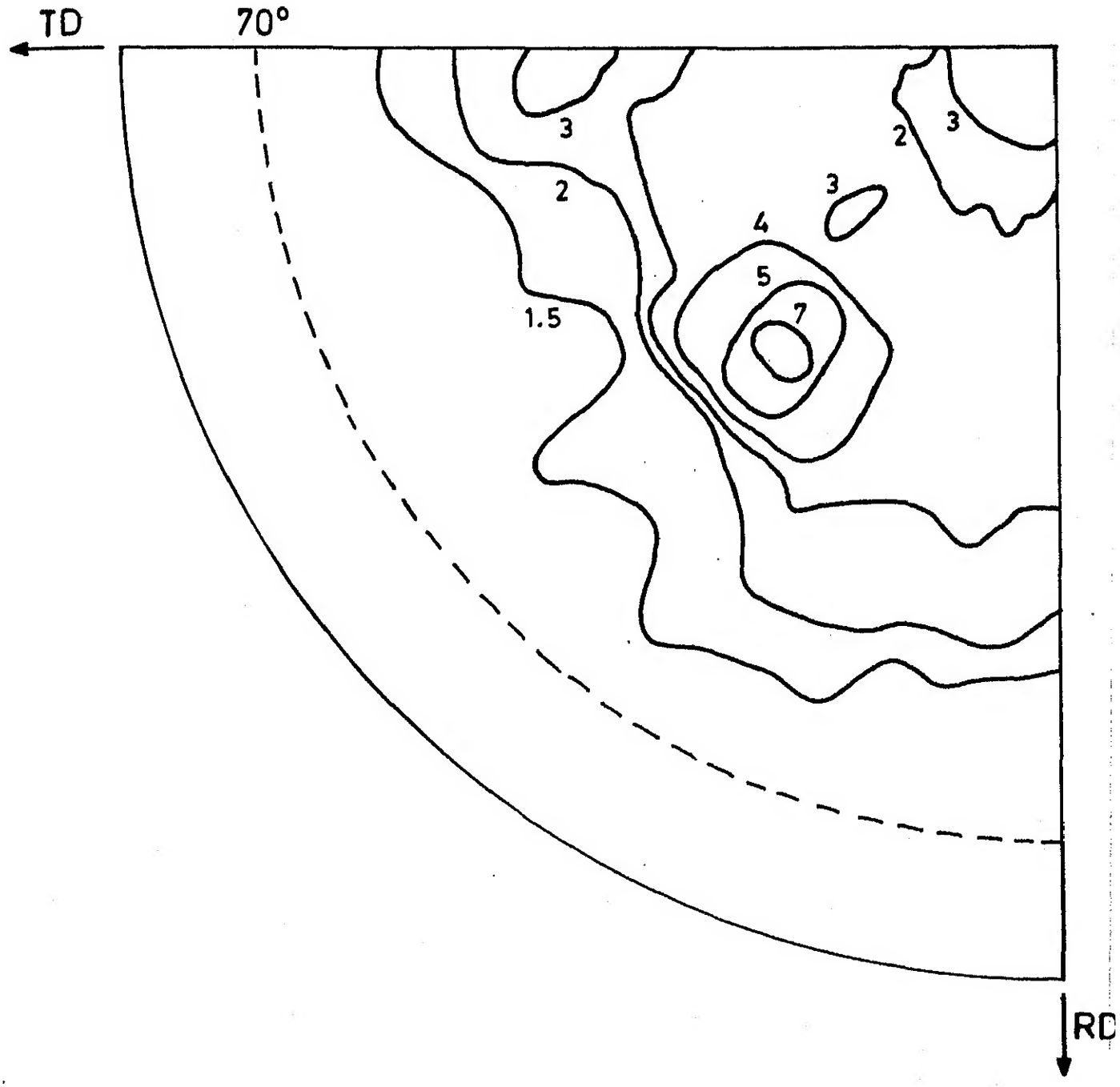

Fig. 4.4 (b) (111) pole figure of precipitation-treated alloy, deformed 90% and then heated to 300°C for 1hr.

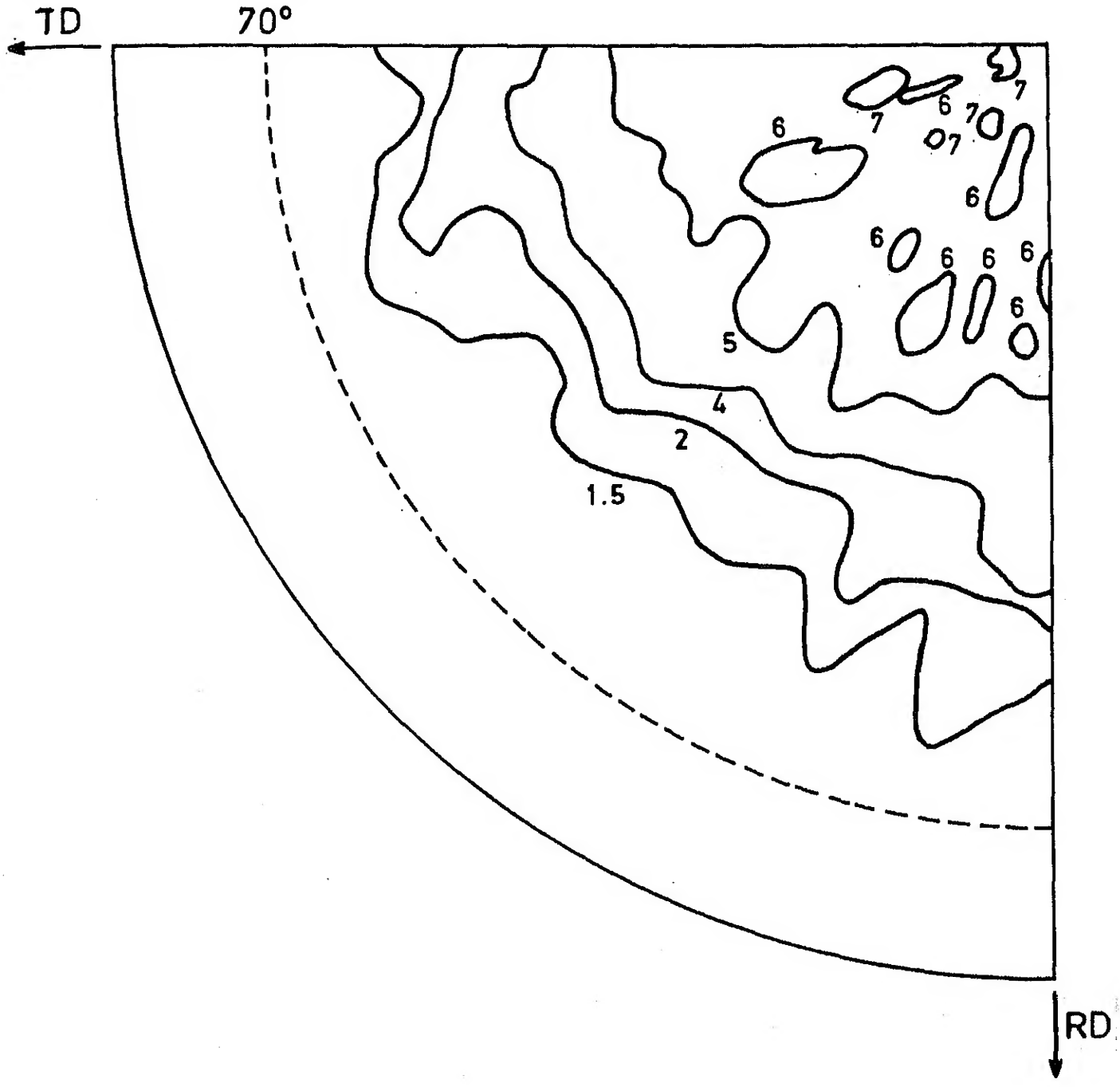

Fig. 4.4 (c) (111) pole figure of precipitation-treated alloy, deformed 90% and then heated to 350°C for 1hr.

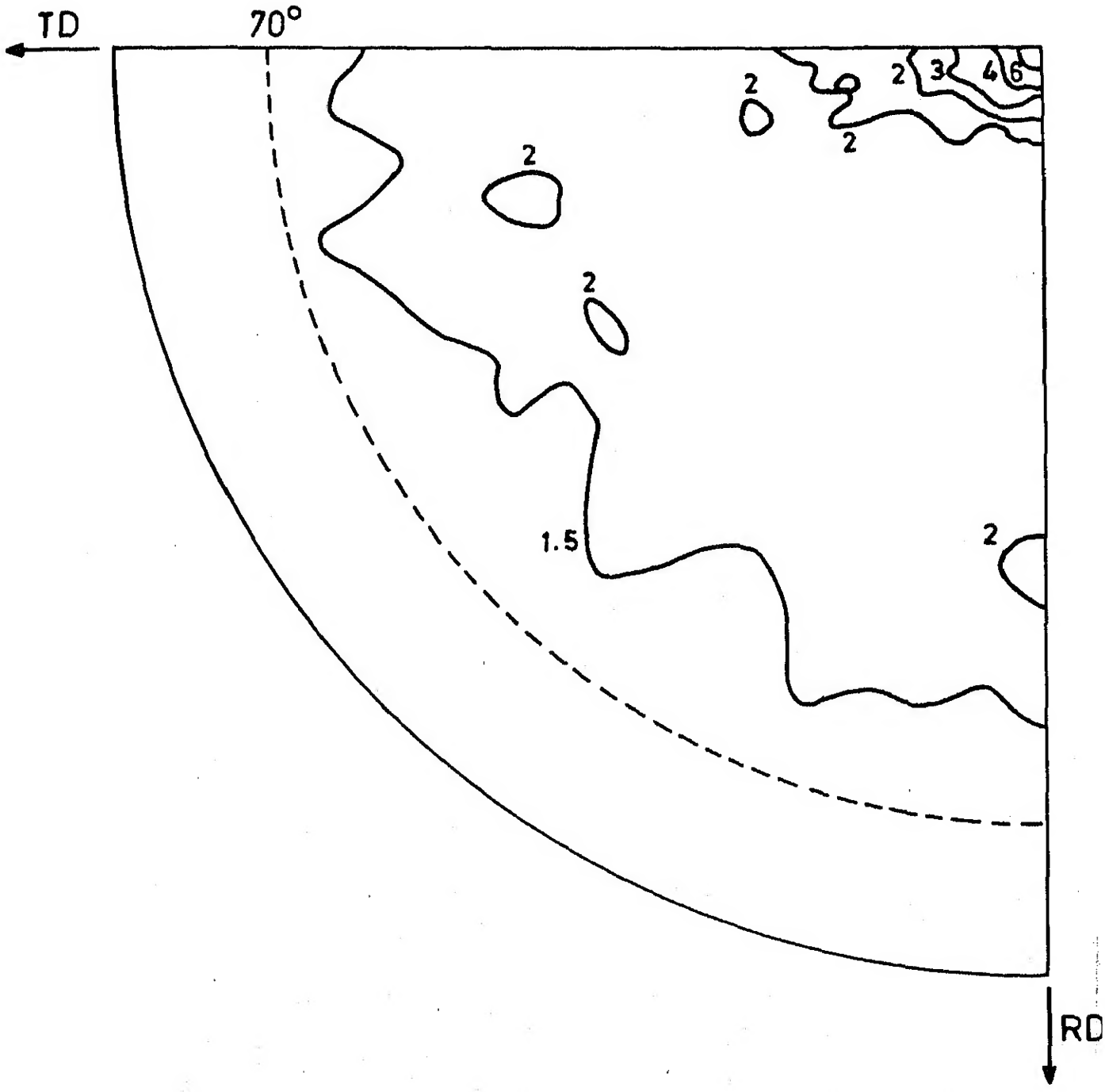

Fig. 4.5 (111) pole figure of precipitation-treated alloy, deformed 60 %.

4.3 Electron Microscopic Studies

Electron microscopic studies have been carried out on the cold-worked as well as annealed samples for both the solution-treated and precipitation-treated alloys. The results are discussed below.

4.3.1 Nature of Precipitating Phases: A number of selected area diffraction patterns have been taken from the precipitate particles after various treatments to determine the nature of the particles. Diffraction patterns have been taken from the solution-treated alloy also to check for any possible presence of precipitate particles. The patterns are indexed by camera constant and ratio technique methods.

Figures 4.6(a) and (b) show the diffraction patterns of the matrix taken after the solution treatment at 620°C for 24 hrs. The pattern in Fig. 4.6(a) can be indexed for α-aluminium solid solution with the electron beam direction $[\bar{1}23]$. The details of indexing are shown in the figure. The pattern in Fig. 4.6(b) also can be indexed for α-aluminium solid solution with the electron beam direction $[\bar{0}01]$. These two figures along with the absence of any particle in the micrographs establish the fact that the alloy is single phase after this treatment and that all the managanese is in solid solution in aluminium.

Figures 4.7(a) to (g) show the diffraction patterns of the precipitate particles obtained after various treatments.

The particles are identified as $MnAl_6$, C-centred orthorhombic with lattice parameters, a = 6.504 A°, b = 7.555 A° and c = 8.864 A° (2). All the patterns have been tried for indexing for the metastable phases, G' (simple cubic, a = 12.75 A°) and G_1 (BCC, a = 7.533 A°) reported to be present, by several authors (47,48) in aluminium manganese alloys at lower temperature of annealing. But a careful indexing of the patterns confirms that they can be indexed for $MnAl_6$ particles only.

Figures 4.7(a) and (b) show the diffraction patterns of particles obtained after the precipitation treatment at 400°C for 2 h followed by 60% and 40% cold deformation. Both the patterns are indexed for $MnAl_6$ with electron beam directions $[1\bar{1}0]$ and $[1\bar{1}\bar{2}]$ respectively. Since the cold working after the 400°C heat treatment is not expected to significantly affect the precipitate particles, the patterns indicate the presence of $MnAl_6$ after the precipitation treatment. The presence of $MnAl_6$ particles have been reported by Gatto et al. (19) and Bleck (36) after the precipitation-treatment of Al-1.04% Mn at 560°C for 48 h and of commercial purity aluminium at 500°C for 200 h respectively. These results indicate that though some metastable phases may be present in Al-Mn alloys at lower temperature of annealing, $MnAl_6$ is the only phase stable at higher temperature.

Fig.4.6 (a)
Matrix; $\vec{B}$ [$\bar{1}$23]

Fig.4.6 (b)
Matrix; $\vec{B}$ [001]

Fig.4.7 (a)
$MnAl_6$; $\vec{B}$ [1$\bar{1}$0]

Fig. 4.6 (a) & (b) : Diffraction patterns obtained from the solution-treated alloy

Fig.4.7 : Diffraction patterns obtained from the precipitate particles in cold-deformed and annealed alloy.

(a) : Precipitation-treated and 60% deformed.

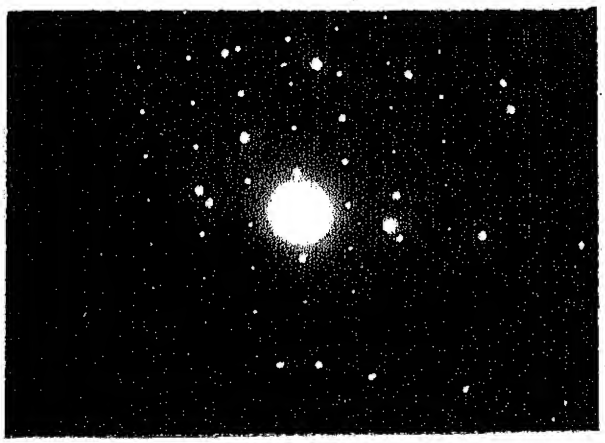

Fig. 4.7 (b)
$MnAl_6$; $\vec{B}$ [1$\bar{1}\bar{2}$]

Fig. 4.7 (c)
$MnAl_6$; $\vec{B}$ [$\bar{3}$12]

Fig.4.7 (d)
$MnAl_6$; $\vec{B}$ [$\bar{1}$1$\bar{1}$]

Fig.4.7 (b) : Precipitation-treated and 40% deformed.
(c) & (d) : Precipitation-treated, 60% deformed and annealed at 250°C for 1 h .

Fig. 4.7 (e)
$MnAl_6$; $\vec{B}$ [$\bar{3}$14]

Fig. 4.7 (f)
$MnAl_6$; $\vec{B}$ [$\bar{1}$1$\bar{2}$]

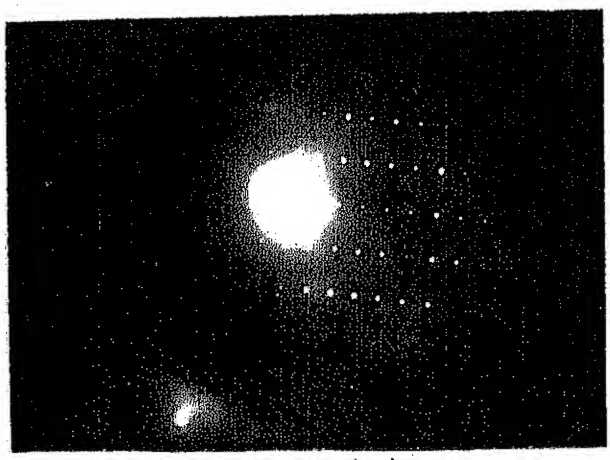

Fig.4.7 (g)
$MnAl_6$; $\vec{B}$ [1$\bar{1}$0]

Fig.4.7 (e) : Precipitation-treated, 60% deformed and annealed at 300°C for 1 h .
(f) : Precipitation-treated, 60% deformed and annealed at 350°C for 1 h .
(g) : Solution-treated, 60% deformed and annealed at 350°C for 1 h .

Figures 4.7(c) to (f) are the diffraction patterns of the precipitate particles obtained after the cold working of precipitation-treated alloy followed by annealing at 250°C, 300°C and 350°C for 1 h each. Here also the patterns have been indexed for $MnAl_6$ particles — the details of indexing being shown in respective figures. These patterns indicate that the particles formed during the precipitation treatment have been retained after the subsequent annealing treatments.

Figure 4.7(g) shows the diffraction pattern of the particle obtained from the 60% cold deformed solution-treated alloy after an annealing treatment of 350°C for 1 h. This also can be indexed for $MnAl_6$ only with electron beam direction $[1\bar{1}0]$.

4.3.2 Microstructural Studies: Figures 4.8 to 4.20 show the microstructure of the solution-treated and precipitation-treated alloys under various conditions.

4.3.2.1 Solution-treated Alloy: The solution-treated alloy shows well-defined cell structure after 90% cold deformation (Figs. 4.8(a) and (b)). The average cell size is $\sim 0.9\ \mu m$. The same alloy, after 60% deformation also shows well-defined cell structure (Figs.4.9a and b) with average cell size 1.05μm. A comparatively weaker cell structure with average cell size $\sim 1.3\ \mu m$ dominates after 40% cold deformation

(Figs. 4.10 a and b). The cell interiors are relatively free from dislocations, whereas the walls are regions of high dislocation density.

The appearance of cell structure in aluminium alloys after cold deformation is very common and is attributed to the high stacking fault energy of the material which helps the screw dislocations to cross-slip out of their original slip planes and to arrange themselves in very localized regions which form the cell walls. The cell sizes show a gradual increase in size with decrease in percent deformation and this is in good-agreement with the literature (13).

The results obtained in this case in terms of the weakening of cell structure with decrease in percent deformation is consistent with the results reported by Gatto et al (19). They worked on the commercial purity aluminium containing 1.04% Mn and found that the material is characterized by isolated dislocation tangles after 10% deformation, weak cell structure after 30% deformation and well defined cell structure beyond 50% cold deformation.

The cellular structure prevails in case of 60% deformed solution-treated alloy after annealing at 250°C for 1 h (Fig.4.11 a and b). A slight change in dislocation arrangements is noteworthy. The cell interiors are completely free from any dislocation. This suggests the starting of the recovery process in the alloy. No precipitate particle

has been seen under the microscope at this stage.

The solution-treated alloy exhibits recovered structure in general after annealing at 300°C for 1 h . Figs. 4.12 (a) and (b) show the microstructure of the 90% deformed alloy after the annealing treatment. The structure is characterized by the presence of subgrains of mean size ~ 1.3 μm. The 60% deformed alloy also exhibits subgrain structure after this treatment (Figs. 4.13 a to c). The subgrains are of mean size ~ 1.5 μm. The presence of high angle boundaries shows the starting of the recrystallization process. The subgrains show a regular morphology with dislocation free interior regions. Some small dots are seen in the figures which are probably due to the precipitate-particles. Due to the very fine size of them, it was not possible to know the nature by taking selected area diffraction pattern. Fig. 4.13(c) depicts subgrains surrounded by comparatively thinner boundaries. This illustrates the fact that thinning of subgrain boundaries has started in some parts of the sample and is considered as a step towards the nucleation of recrystallized grains.

The results obtained in the present study are similar to that reported by Gatto et al. (19). They observed the thinning of subgrain boundaries to occur in 70% deformed solution-treated alloy after annealing at 300°C for 1 h .

Figures 4.14 (a) and (b) show the microstructure of the 90% deformed solution-treated alloy after annealing at 350°C for 1 h . The micrographs clearly exhibit recrystallized structure without any presence of the previous deformation effect. Precipitate particles are also seen in the micrographs. They are distributed evenly along the grain boundaries and in the grain interiors. Some very fine particles are seen to be lying very close to the dislocations inside the grains (Fig. 4.14 b). The micrographs show the tendency of the precipitate particles for heterogeneous nucleation on grain boundaries and dislocations. Figs.4.15(a) and (b) show the precipitates obtained after the annealing of 60% deformed solution-treated alloy at 350°C for 1 h . The precipitates are again seen to be present on the grain boundary (Fig. 4.15 a) and also inside the grain (Fig.4.15 b). They are globular in shape with mean size of the precipitates is $\sim$ 0.6 μm and density $\sim 5.12 \times 10^{18}/m^3$. The alloy does not show the presence of any deformation effect.

4.3.2.2 Precipitation-treated Alloy: The precipitation-treated alloy also shows cell structure after cold deformation (Figs. 4.16 and 4.17) without any significant change in the cell size compared to their solution-treated counterparts. Figs. 4.16(a) and (b) and 4.17(a) to (d) show the microstructure of the deformed alloy after 40% and 60% deformation respectively. The 60% deformed alloy shows well-defined cell structure, whereas weak cell structure is

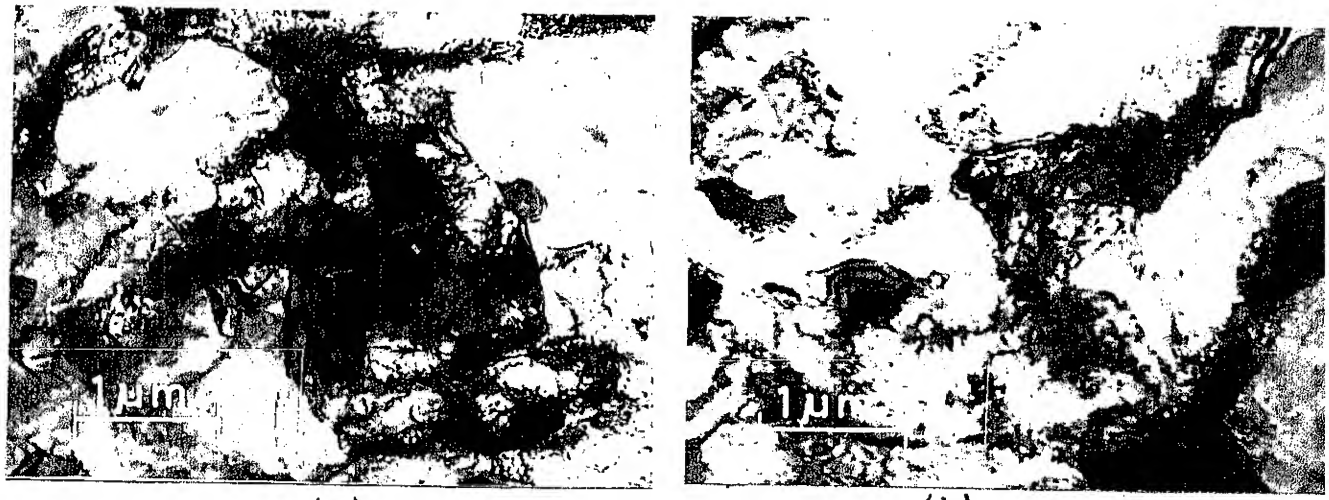

(a) (b)

Fig.4.8 (a) & (b) : Microstructures of solution-treated alloy, deformed 90%

(a) (b)

Fig.4.9 (a) & (b) : Microstructures of solution-treated alloy, deformed 60%

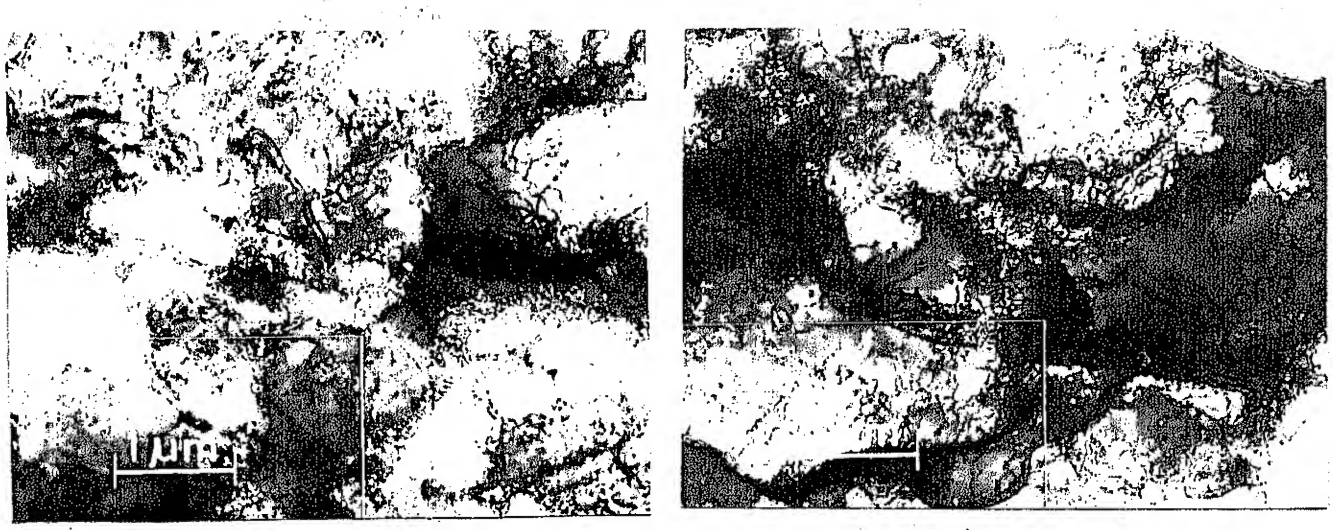

(a) (b)

Fig. 4.10 (a) & (b) : Microstructures of solution-treated alloy, deformed 40%

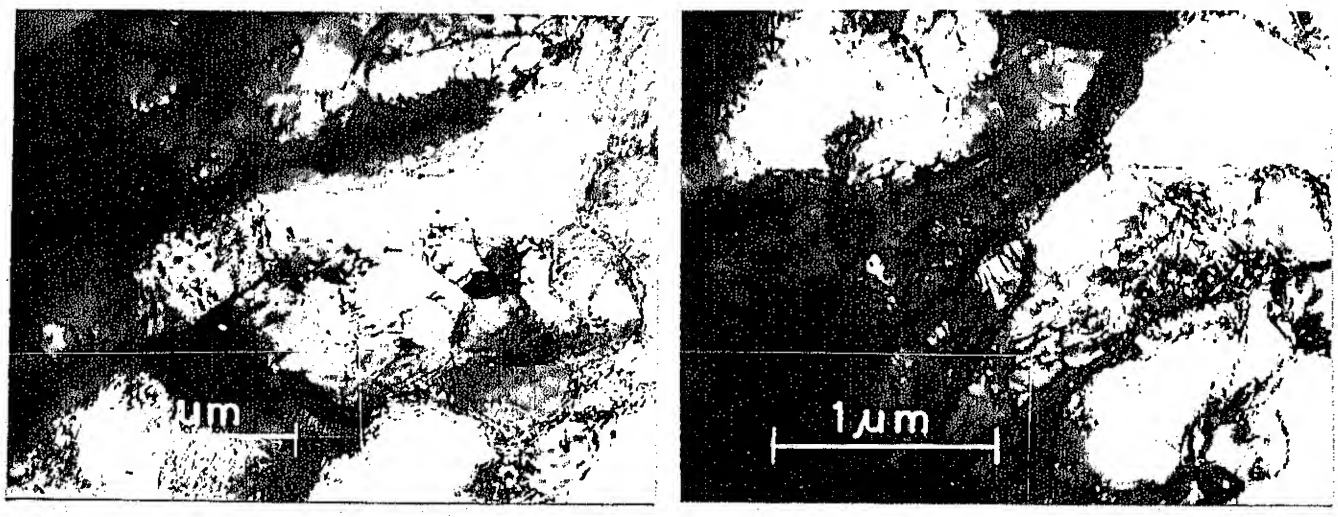

(a) (b)

Fig. 4.11 (a) & (b) : Microstructures of solution-treated alloy, deformed 60% and then annealed at 250°C for 1 h .

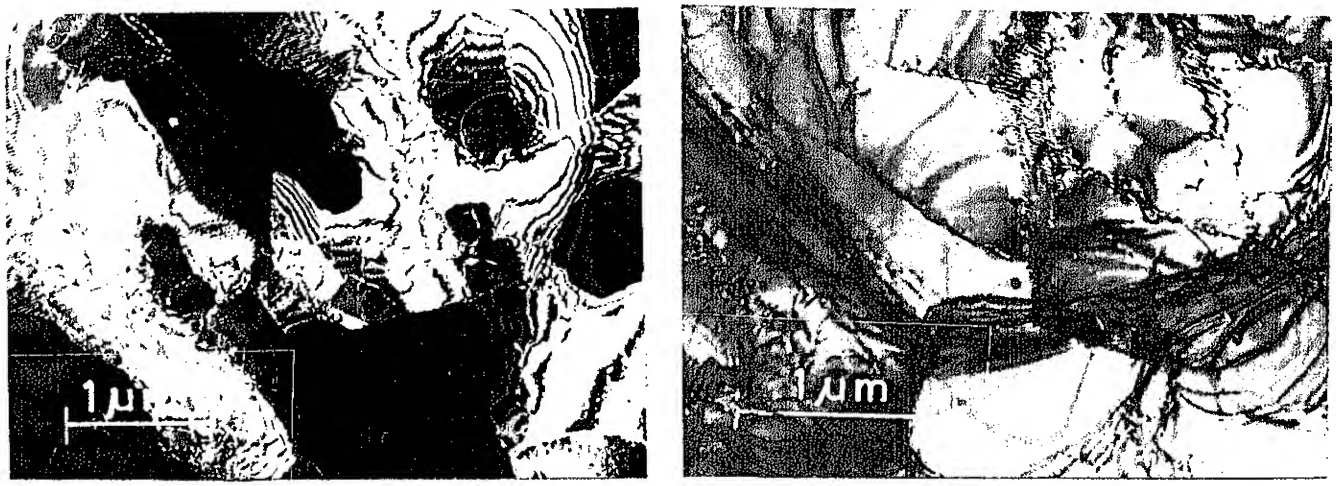

(a) (b)

Fig. 4.12 (a) & (b) : Microstructures of solution-treated alloy, deformed 90% and then annealed at 300°C for 1 h .

(a) (b)

Fig.4.13 (a) to (c) : Microstructures of solution-treated alloy, deformed 60% and then annealed at 300°C for 1 h .

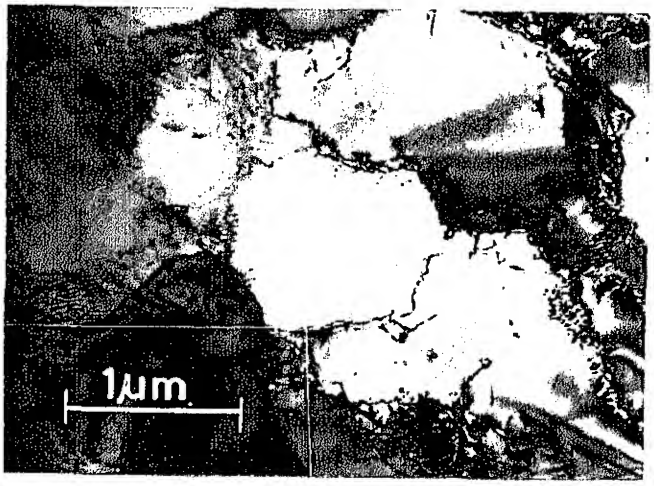

Fig. 4.13 (c)

(a) (b)

Fig.4.14 (a) & (b) : Microstructures of solution-treated alloy, deformed 90% and then annealed at 350°C for 1 h .

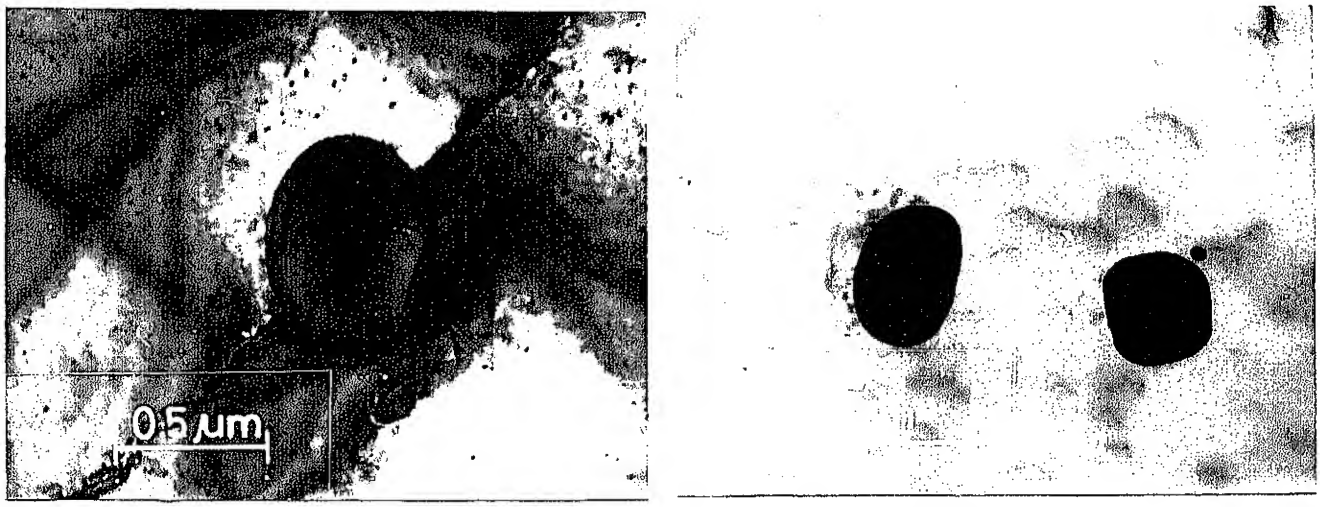

(a) (b)

Fig.4.15 (a) & (b) : Microstructures of solution-treated alloy, deformed 60% and then annealed at 350°C for 1 h .

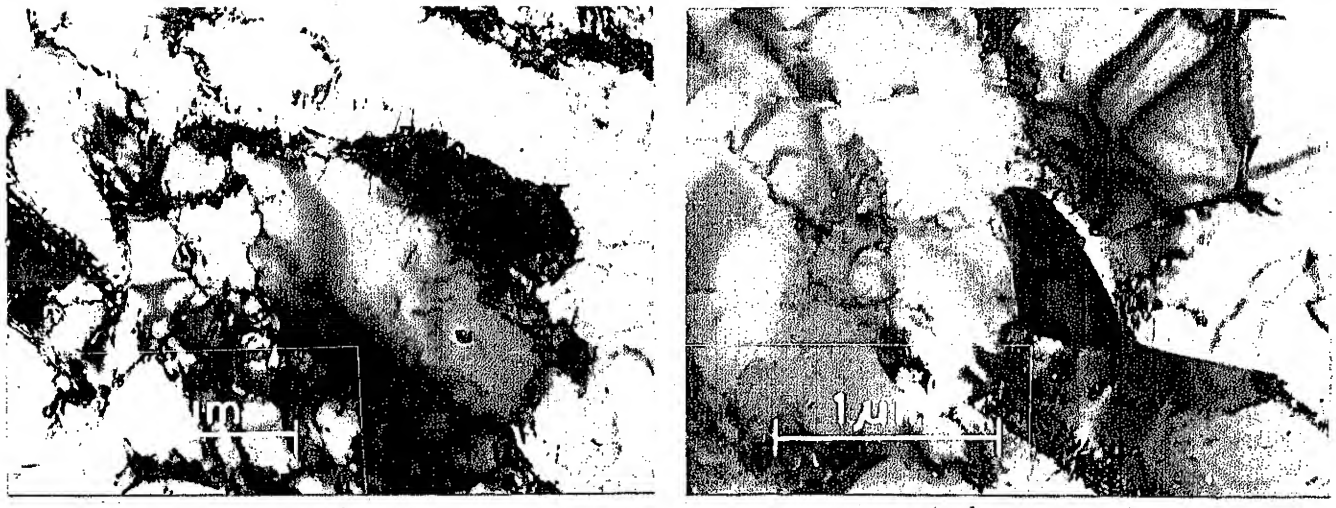

(a) (b)

Fig.4.16 (a) & (b) : Microstructures of precipitation-treated alloy, deformed 40%.
(a) : region away from the particle
(b) : region near the particle.

exhibited by 40% deformed alloy. The alloy shows less tendency towards the formation of cell structure in presence of precipitate particles. This is clear from the comparison between the regions near the precipitate particles and regions free from any particle (Fig. 4.16 a and b) and (Figs. 4.17 a,b and c,d). A careful look of the two regions signifies the difference in structure — very weak cell structure dominates the region near the precipitate particle, whereas the region not containing any precipitate particle is characterized by well-defined cell structure.

The results obtained in this regard is consistent to that predicted in literature. Gatto et al. (19) have also found weaker cell structure for precipitation-treated alloy compared to the solution-treated one and concluded in their paper that normal cell structure occurred at a lower deformation in the solution-treated alloy. The particles are believed to be responsible in hindering the formation of cell structure in deformed materials, when their sizes are below the critical value which stimulates the recrystallization process. In this case the deformation required to initiate a cell structure is usually greater than in the corresponding single phase metal.

The particles obtained after the precipitation treatment at 400°C for 2 hrs. are mostly globular in shape with mean size $\sim$ 0.70 μm and density $5.4 \times 10^{18}/m^3$.

The micrographs 4.18(a) to (c) show the structure of the 60% deformed precipitation-treated alloy after annealing at 250°C for 1 h . Figs. 4.18(a) and (b) depict the cellular structure prevailing after the treatment. The structure is characterised by weak cells with interiors free from any dislocations. Some of the areas exhibit the presence of subgrains of mean size $\sim 1.4\,\mu m$ surrounded by high angle boundaries (Fig. 4.18 c). This micrograph clearly illustrates the starting of the recovery process in some areas. The precipitate particles obtained in this case are mostly globular and plate shaped in nature with no significant change in size and density compared to the starting material.

A comparison between the Figs.4.11(a) and (b) and 4.18(c) indicates that the precipitation-treated alloy has moved a bit forward towards the recyrtsllization process compared to the solution treated alloy after annealing at 250°C for 1 h .

Figures 4.19(a) and (b) depict the structure of the 60% deformed alloy after annealing at 300°C for 1 h . The micrographs are characterized by small recrystallized grains in almost all regions without any effect of the previous deformation being present. A comparison between the solution-treated and precipitation-treated states of the alloy at this stage illustrates that the solution-treated alloy exhibits recovered structure after this treatment (Figs.4.13 a to c), whereas fully recrystallized structure is exhibited by

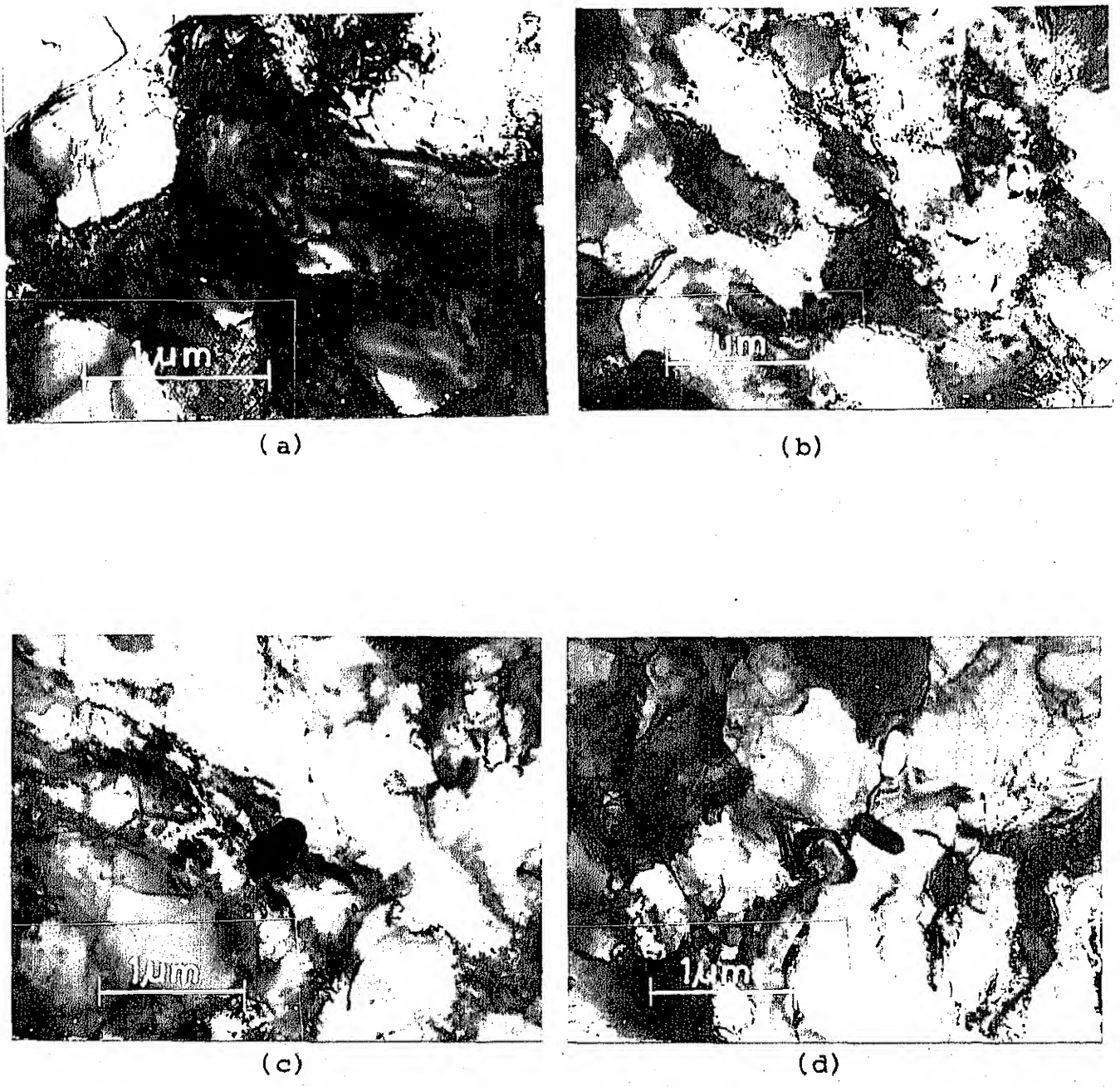

(a) (b)

(c) (d)

Fig. 4.17 (a) to (d) : Microstructures of precipitation-treated alloy, deformed 60%.
(a) & (b) : region away from the particle
(c) & (d) : region near the particle.

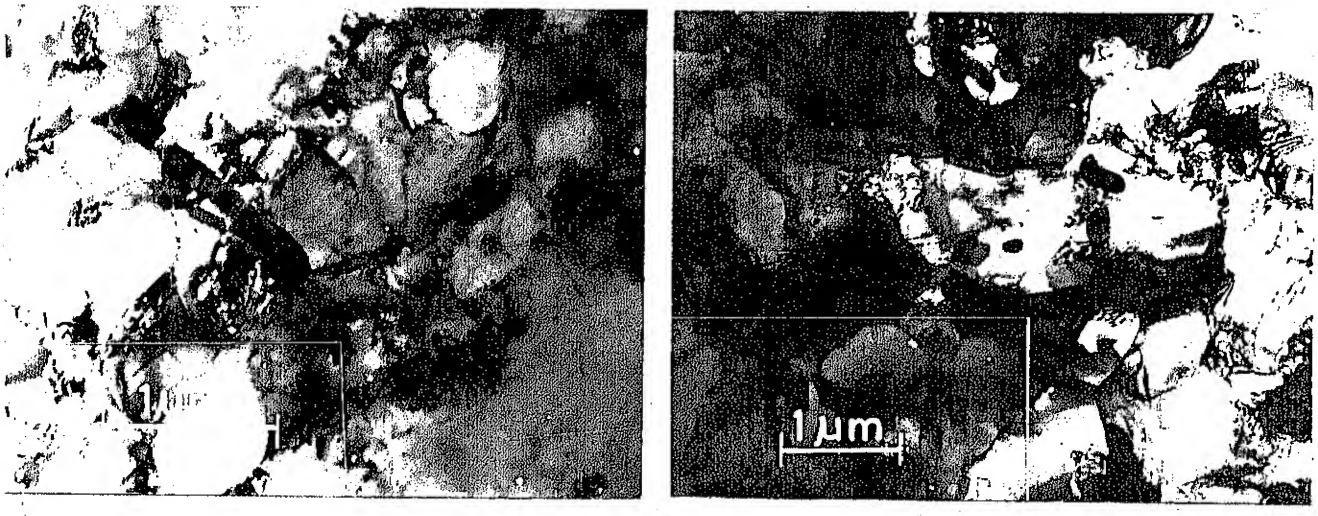

(a) (b)

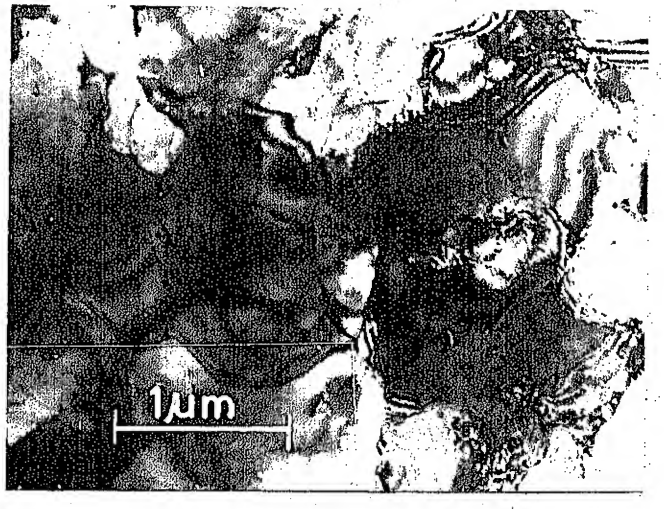

(c)

Fig.4.18 (a) to (c) : Microstructures of precipitation-treated alloy, deformed 60% and then annealed at 250°C for 1 h .

(a) (b)

Fig.4.19(a) & (b) : Microstructures of precipitation-treated alloy, deformed 60% and then annealed at 300°C for 1 h .

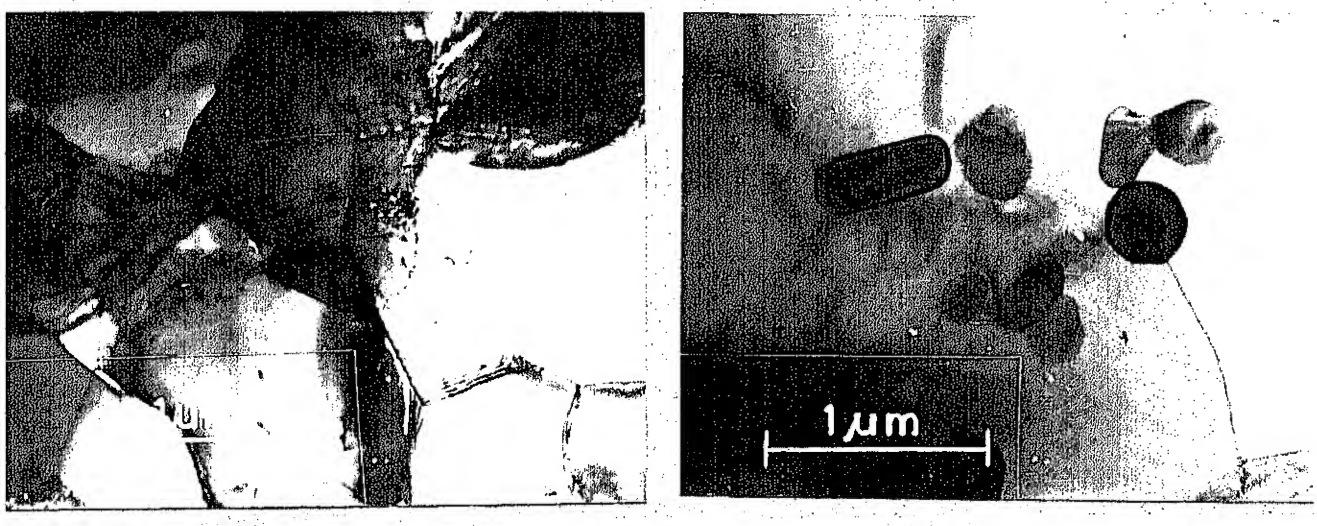

(a) (b)

Fig.4.20(a) & (b) : Microstructures of precipitation-treated alloy, deformed 60% and then annealed at 350°C for 1 h.

the precipitation-treated alloy.

Figures 4.20(a) and (b) reveal the microstructure of the 60% deformed precipitation-treated alloy after annealing at 350°C for 1 h . The alloy shows recrystallized grains after this treatment. A comparison between this structure and that obtained after annealing at 300°C for 1 h (Figs. 4.19 a and b) clearly indicates that some grain coarsening has taken place after this treatment. The precipitates obtained at this stage are again globular in shape with no change in size and density compared to the starting material.

4.4 General Discussion:

Solution treatment of the alloy at 620°C for 24 h leads to the complete dissolution of manganese and water quenching from this temperature results in a supersaturated solid solution. There is evidence (19,50) to suggest that the amount of dissolved manganese controls the recrystallization process — the higher the amount of dissolved manganese, the more difficult is the recrystallization process.

The primary step in recrystallization is the movement of low and high angle boundaries. Precipitation on to the recrystallization front during or before the movement of the boundary is an important factor controlling the recrystallization process. The interaction between

precipitation and recrystallization can be explained by the time-temperature diagram shown in Fig. 4.21 (51,52). At high temperatures, the recrystallization process is completed before the onset of precipitation (Region I). When the rates of precipitation and recrystallization are comparable (Region II), the two processes occur simultaneously and the mobility of the recrystallization front is adversely affected by the precipitate particles. At the time of precipitation the particles are very small in size and they retard the recrystallization process by pinning the boundary migration. In region III, precipitation precedes recrystallization and if the particle size and interparticle spacing are below the critical level, the recrystallization process gets retarded.

The retarding force for recrystallization is provided by the particles which hinder the movement of the recrystallization front. This force is directly proportional to the volume fraction of the precipitate and inversely to the size. For a given volume fraction of the precipitate particles, the retarding force is appreciable in the early stages of precipitation due to small size of the particles. However, when the particles begin to grow, the retarding force is reduced and the mobility of the recrystallization front is increased.

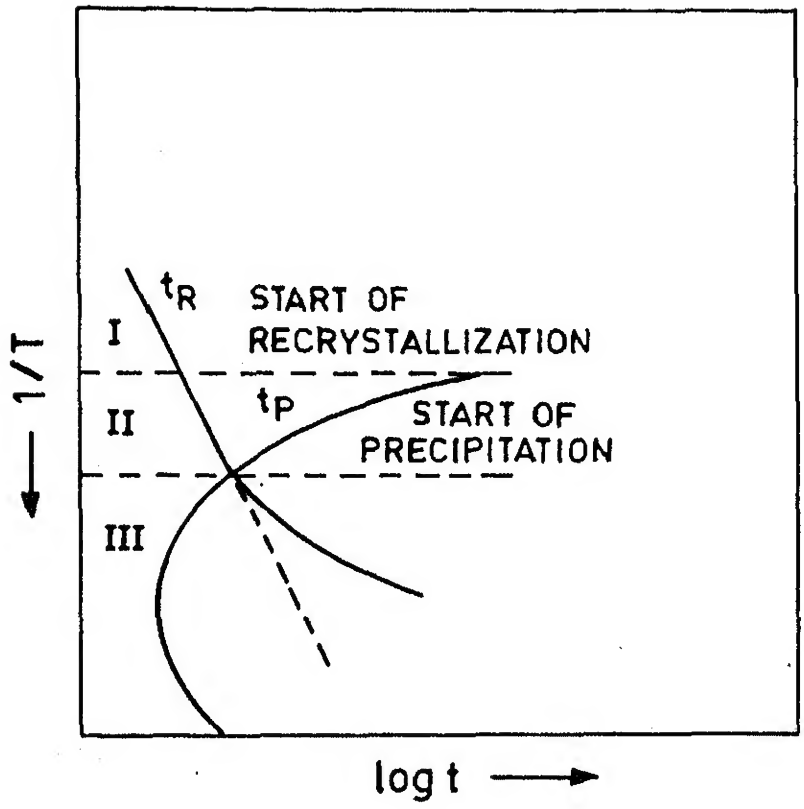

Fig. 4.21 Interaction between recrystallization and precipitation.

It has been found in the present investigation that the 60% deformed precipitation-treated alloy shows complete recrystallization after annealing at 300°C for 1 hr (Fig. 4.19), whereas the solution-treated alloy exhibits recovered structure (Fig. 4.13) after the same treatment. This indicates clearly that the precipitation-treated alloy shows more favourable response to recrystallization. The same type of result has been obtained by texture analysis in case of 90% deformed samples, where the precipitation-treated alloy shows recrystallized texture after annealing at 300°C for 1 hr (Fig. 4.4 b) and the solution-treated alloy shows the presence of rolling texture component after the same treatment (Fig. 4.1 b). There is enough experimental evidence (26-29) to suggest that the critical size of the particle which stimulates the recrystallization process is about 1 μm. Since the particle size of the precipitation treated alloy is ~0.7 μm, the result obtained in the present investigation cannot be described as the effect of particle stimulated recrystallization. On the other hand, precipitation from the deformed solution-treated samples may occur at lower annealing temperatures (50) and the increase in recrystallization temperature for the solution-treated alloy can be described in terms of the interaction between the recrystallization and precipitation processes. When

the two processes occur simultaneously, then the recrystallization process gets delayed due to the small size of the particles at the initial stages of precipitation. The small precipitate particles are believed to pin the subgrain boundary migration and thereby retard the recrystallization process. Very small particles have been observed in case of the solution-treated alloy after annealing at 300°C for 1 hr (Fig. 4.13).

The cell size of the deformed structure exhibits an increase in size with decrease in percent deformation. The cell sizes of the solution-treated alloy are about 0.9 μm, 1.05 μm and 1.3 μm after 90%, 60% and 40% cold deformation respectively. The result obtained in this case is similar to that reported by Gatto et al. (19) who observed well defined cell structure of size ~ 1 μm after 90% deformation in case of Al-1.04% Mn alloy.

The cell size does not show any significant change in the precipitation treated alloy compared to its solution-treated counterpart. But the regions near the precipitate particles show weaker cell structure and the regions away from the particles exhibit well-defined cell structure. This has been reported by Gatto et al. (19). They attributed the weakening of cell structure to the hindering effect played by the precipitate particles during cell formation.

The recrystallized grain size is about ~1.5 μm after the annealing of the 90% deformed solution-treated alloy at 350°C for 1 h. The grain size of the 60% deformed alloy is about ~ 2.9 μm after the same treatment. This gives clear indication of the dependence of recrystallized grain size on the amount of deformation; with the increase of percent deformation the recrystallized grain size decreases.

CHAPTER 5

CONCLUSIONS

(1) The superpurity Al-1.0% Mn alloy exhibits cell structure in general after cold working. The cell size increases with decrease in percent deformation.

(2) The precipitation-treated alloy shows weaker cell structure in regions near the precipitate particles compared to that away from the precipitate particles.

(3) Precipitation from the supersaturated solid solution occurs at 300°C after both 90% and 60% deformation.

(4) The recrystallization process is hindered in solution-treated alloy. The precipitation-treated alloy shows full recrystallization after annealing at 300°C for 1 h, whereas the solution-treated alloy predominantly shows subgrains after the same treatment.

(5) The rolling texture is retained by the 90% deformed solution-treated alloy after annealing at 300°C for 1 h. But the precipitation-treated alloy exhibits recrystallization texture after the same treatment.

(6) The alloy shows varying rolling texture on deformation with (111) [uvw], (111)[$\bar{1}$12] , (123) [41$\bar{2}$] and (332) [11$\bar{3}$] orientations.

(7) The alloy exhibits random texture after recrystallization with a slight preference for the (023) $[33\bar{2}]$ orientation.

(8) The recrystallized grain size decreases with increase in percent deformation. The grain size of the 90% deformed alloy is about ~1.5 μm after annealing at 350°C for 1 h and for the 60% deformed alloy the grain size is about ~2.9 μm.

REFERENCES

1. L.F. Mondolfo, 'Manganese in Aluminium Alloys', Manganese Centre, Paris, p. 1.

2. L.F. Mondolfo, 'Aluminium Alloys: Structure and Properties', Butterworths, London, p. 324.

3. L.F. Mondolfo, 'Aluminium Alloys: Structure and Properties', p. 325.

4. L.F. Mondolfo, 'Manganese in Aluminium Alloys', p. 93.

5. L.F. Mondolfo, 'Aluminium Alloys: Structure and Properties', p. 97.

6. L.F. Mondolfo, 'Manganese in Aluminium Alloys', p.37.

7. L.F. Mondolfo, 'Manganese in Aluminium Alloys', p. 38.

8. L.F. Mondolfo, 'Manganese in Aluminium Alloys', p. 40.

9. L.F. Mondolfo, 'Manganese in Aluminium Alloys', p.42.

10. L.F. Mondolfo, 'Manganese in Aluminium Alloys', p.46.

11. L.F. Mondolfo, 'Manganese in Aluminium Alloys', p. 49.

12. R.D. Heidenreich, J. Appl. Phys. 20 (1949) 993.

13. P. Cotterill and P.R. Mould, 'Recrystallization and Grain Growth in Metals', p.12.

14. P.R. Swann, 'Electron Microscopy and Strength of Crystals', ed. G. Thomas and J. Washburn, Interscience, New York, 1963, p.131.

15. S. Weissman, T. Imura and N. Hosokawa, 'Recovery and Recrystallization in Metals', ed. L. Himmel, Interscience, New York, 1963, p. 246.

16. P. Cotterill and P.R. Mould, 'Recrystallization and Grain Growth in Metals', p.19.

17. P. Gay, P.B. Hirsch and A. Kelly, Acta Crystallogr., 7 (1954) 41.

18. P. Cotterill and P.R. Mould, 'Recrystallization and Grain Growth in Metals', p. 21.

19. F. Gatto, G. Camona, M. Conserva and P. Fiorini, 'Deformation Structures and Recrystallization Behaviour of Al-1.04% Mn Alloy', Mat. Sci. Engg., 3 (1968-69) 56.

20. B. Bay and N. Hansen, 'Recrystallization in Commercially Pure Aluminium', Met. Trans., 15A (1984) 287.

21. J. Grewen, T. Noda and D. Saner, Z. Metallk., 68 (1977) 260.

22. I.L. Dillamore, P.L. Morris, C.J.E. Smith and W.B. Hutchinson, Proc. Roy. Soc., London, A 329 (1972) 405.

23. P. Cotterill and P.R. Mould, 'Recrystallization and Grain Growth in Metals', p. 140.

24. E. Grant, A. Porter and B. Ralph, 'Grain Boundary Migration in Single Phase and Particle Containing Materials', J. Mat. Sci., 19 (1984) 3554.

25. E. Nes, 'The Effect of a Fine Particle Dispersion on Heterogeneous Recrystallization', Acta Met., 24 (1976) 391.

26. F.J. Humphreys, 'Recrystallization Mechanism in Two Phase Alloys', Met. Sci., 13 (1979), 136.

27. F.J. Humphreys, 'The Nucleation of Recrystallization at Second Phase Particles in Deformed Aluminium', Acta Met., 25 (1977) 1323.

28. F.J. Humphreys, 'Nucleation of Recrystallization in Metals and Alloys with Large Particles', Proc. 1st Riso Int. Symposium on Metallurgy and Materials Science, Riso National Laboratory, Roskilde, Denmark (1980), p. 35.

29. L.M. Brown and R.K. Ham, 'Dislocation-particle Interactions', In : Strengthening Methods in Crystals, ed. A. Kelly and R.B. Nicholson, p.9.

30. A.R. Jones and N. Hansen, 'Recovery Changes Leading to Nucleation of Recrystallization', Proc. 1st Riso Int. Symposium on Metallurgy and Materials Science, Rs Riso National Laboratory, Roskilde, Denmark (1980); p.13.

31. H.M. Chan and F.J. Humphreys, 'Effect of Particle Stimulated Nucleation on Orientation of Recrystallized Grains, Met. Sci., 18 (1984) 527.

32. J.R. Porter and F.J. Humphreys, 'Nucleation of Recrystallization at Second Phase Particles in Deformed Copper Alloys', Met. Sci., 13 (1979) 83.

33. R. Sandström, 'Formation and Growth of Recrystallization Nuclei around Particles', Z. Metallk., 71 (1980) 681.

34. R. Sandström, 'Criteria for Nucleation of Recrystallization around Particles', Proc. 1st Riso Int. Symposium on Metallurgy and Materials Science, Riso National Laboratory, Roskilde, Denmark (1980), p. 45.

35. R. Sandström, 'Subgrain Growth Occurring by Boundary Migration', Acta Met., 25 (1977) 905.

36. W. Bleck and H.J. Bunge, 'The Recrystallization of AlMn 1 investigated with Pole Figures by Number', Acta Met., 29 (1981) 1401.

37. W. Heye and G. Wassermann, Z. Metallk., 59 (1968) 617.

38. I.L. Dillamore and N.S. Stolloff, 'Texture Development under Conditions of Imposed Strain; the Influence of Stacking Fault Energy and Degree of Order', in 'Textures in Research and Practice', (ed. J. Grewen and G. Wassermann), Berlin, Springer-Verlag (1969), p.110.

39. I.L. Dillamore and W.T. Roberts, Acta Met., 12 (1964), 281.

40. W. Bunk, Z. Metallk., 56 (1965) 645.

41. F. Lihl and W. Pexa, Z. Metallk., 58 (1967) 465.

42. R. Sundberg, 'The Occurrence of a 'Brass-type' Texture in Aluminium', in 'Textures in Research and Practice', (ed. J. Grewen and G. Wassermann), Berlin, Springer-Verlag (1969), p. 130.

43. A.L. Dons and E. News, 'Nucleation of Cube Texture in Aluminium', Mat. Sc. & Tech., 2 (1986) 8.

44. P. Herbst and J. Huber, in Proc. 5th Int. Conf. on 'Texture' (ed. G. Gottstein and K. Lucke), Berlin, Springer-Verlag (1978), p. 453.

45. J. Grewen, Metall., 19 (1965) 212.

46. A.M. Gokhale, 'Estimation of Average Size of Convex Particles', Met. Trans. 4A (1986).

47. B.D. Cullity, 'Elements of X-ray Diffraction', p.290.

48. R. Hoier, S.E. Naess and E. Nes, Z. Metallk., 64 (1973) 640.

49. G. Hausch, P. Furrer and H. Warlimont, Z. Metallk., 69 (1978) 174.

50. D.B. Goel, P. Furrer and H. Warlimont, Aluminium, 50 (1974) 511.

51. U. Koster, Met. Sci., 8 (1974) 151.

52. K. Lucke and H.P. Stuwe, Acta Met., 19 (1971) 1087.

APPENDIX I

INTERPLANAR SPACINGS (d) FOR THE VARIOUS PHASES

Table A-I.1 Al_6Mn (C-Centred Orthorhombic)
a = 6.504 Å, b = 7.555 Å, c = 8.864 Å

hkl	d(Å)	hkl	d(Å)	hkl	d(Å)
001	8.860	131	2.269	313	1.703
110	4.925	004	2.217	115	1.668
002	4.437	203	2.187	224	1.648
111	4.307	222	2.153	330	1.643
020	3.777	310	2.081	240	1.631
021	3.470	132	2.077	400	1.626
112	3.290	311	2.028	331	1.616
200	3.246	114	2.020	134	1.612
201	3.052	024	1.912	241	1.606
003	2.950	223	1.893	025	1.604
022	2.875	040	1.889	401	1.599
202	2.621	312	1.886	043	1.591
113	2.535	041	1.847	205	1.557
220	2.462	133	1.838	332	1.541
221	2.373	204	1.831	242	1.533
130	2.346	005	1.773	402	1.527
023	2.320	042	1.738	314	1.518
				420	1.494

Table A-I.2 G'-(Simple Cubic)

a = 12.75 Å

hkl	d(Å)	hkl	d(Å)	hkl	d(Å)
001	12.750	024	2.850	006	2.125
011	9.015	124	2.782	016	2.096
111	7.361	233	2.718	235	2.068
002	6.375	224	2.602	116	2.068
012	5.701	034	2.550	026	2.016
112	5.205	005	2.550	344	1.991
022	4.507	134	2.500	045	1.991
003	4.250	015	2.500	126	1.991
122	4.250	333	2.453	145	1.967
013	4.031	115	2.453	335	1.944
113	3.844	234	2.367	226	1.922
222	3.680	025	2.367	245	1.901
023	3.536	125	2.328	036	1.901
123	3.407	044	2.253	136	1.880
004	3.187	144	2.219	444	1.840
014	3.092	225	2.219	236	1.821
223	3.092	334	2.186	007	1.821
114	3.005	035	2.186	345	1.803
033	3.005	135	2.155	055	1.803
133	2.925	244	2.125	017	1.803

Table A-I.3 G_1(BCC) a = 7.533 Å

($Al_{12}Mn$)

hkl	d(Å)	hkl	d(Å)
110	5.327	134	1.477
002	3.767	251	1.375
112	3.075	044	1.332
022	2.663	343	1.292
103	2.382	305	1.292
222	2.175	244	1.256
132	2.013	325	1.222
004	1.883	206	1.191
114	1.776	415	1.162
033	1.776	444	1.087
042	1.684	345	1.065
233	1.606	055	1.065
224	1.538	336	1.025
015	1.477	264	1.007

APPENDIX - II

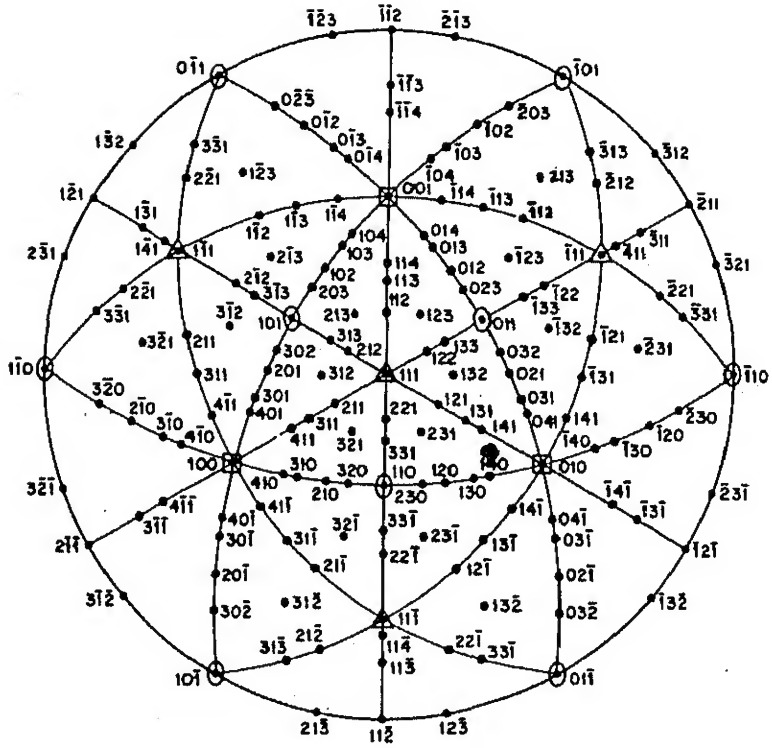

(111) Standard projection of cubic crystal.

APPENDIX-III

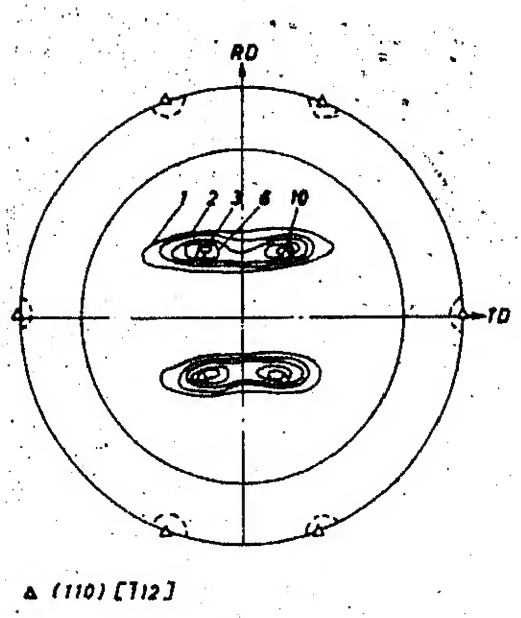

A-III.1 (111) Pole Figure showing (110) [1̄12] Orientation

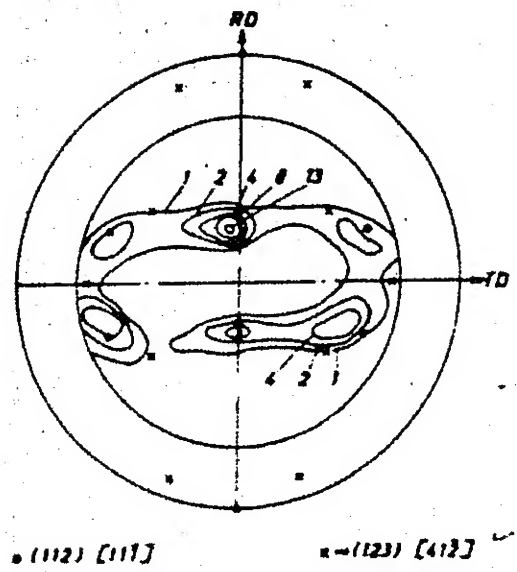

A-III.2 (111) Pole Figure showing (123) [41$\bar{2}$] Orientation.